MICRO-FABRICATION OF A MACH-ZEHNDER INTERFEROMETER COMBINING LASER DIRECT WRITING AND FOUNTAIN PEN MICROPATTERNING FOR CHEMICAL/BIOLOGICAL SENSING APPLICATIONS

Ajay Kallur, B.E.

Thesis Prepared for the Degree of

MASTER OF SCIENCE

UNIVERSITY OF NORTH TEXAS

May 2009

APPROVED:

Shuping Wang, Major Professor
Vijay Vaidyanathan, Committee Member
Nourredine Boubekri, Chair of the Department of Engineering Technology
Costas Tsatsoulis, Dean of the College of Engineering
Michael Monticino, Interim Dean of the Robert B. Toulouse School of Graduate Studies

Kallur, Ajay. Micro-fabrication of a Mach-Zehnder interferometer combining laser direct writing and fountain pen micropatterning for chemical/biological sensing applications. Master of Science (Engineering Systems), May 2009, 106 pp., 2 tables, 31 figures, references, 43 titles.

This research lays the foundation of a highly simplified maskless micro-fabrication technique which involves incorporation of laser direct writing technique combined with fountain pen based micro-patterning method to fabricate polymer-based Mach-Zehnder interferometer sensor arrays' prototype for chemical/biological sensing applications. The research provides methodology that focuses on maskless technology, allowing the definition and modification of geometric patterns through the programming of computer software, in contrast to the conventional mask-based photolithographic approach, in which a photomask must be produced before the device is fabricated.

The finished waveguide sensors are evaluated on the basis of their performance as general interferometers. The waveguide developed using the fountain pen-based micro-patterning system is compared with the waveguide developed using the current technique of spin coating method for patterning of upper cladding of the waveguide. The resulting output power profile of the waveguides is generated to confirm their functionality as general interferometers. The results obtained are used to confirm the functionality of the simplified micro-fabrication technique for fabricating integrated optical polymer-based sensors and sensor arrays for chemical/biological sensing applications.

ACKNOWLEDGEMENTS

I express profound gratitude to my major professor Dr. Shuping Wang for her encouragement, suggestions, invaluable guidance and support throughout this research. Her moral support and continuous guidance enabled me to successfully complete my work. I greatly appreciate her patience and thank her for believing in me.

I am deeply thankful to Dr. Nourredine Boubekri and Dr. Vijay Vaidyanathan for supporting me with work opportunity, encouragement and help with any problems I came across in the engineering technology department.

I am thankful to Total Wire Corporation and Education Foundation Society of Manufacturing Engineers (#R7019) for supporting part of this research project. I appreciate their willingness and interest to help me in this research.

I appreciate the kindness of Dr. Tae-Youl Choi of mechanical energy department for helping me understand and use the fountain pen-based micropatterning system in the small scale instrumentation laboratory for conducting my experiments. I am grateful for his cooperation and willingness to answer questions without hesitation.

I also thank Dr. Robert Hayes for being my thesis committee member and giving his valuable time to guide me and review my thesis. I also thank Dr. Michael Kozak and Dr. Elias Kougianos for their support and guidance in this duration of my master's degree.

I am, as ever, especially indebted to my mother Mrs. Vasudha Kallur, my grandparents K. R. Char and K. Saraswathi bai, my relatives Gopi and Anjali Kallur and my invaluable friend Ms. Harshada Ghodke for their belief, prayers, love and support throughout my life.

TABLE OF CONTENTS

LIST OF TABLES

LIST OF FIGURES

CHAPTER 1

INTRODUCTION

1.1 Introduction to Sensors

Integrated optical (IO) circuits/devices have been used long enough by researchers to develop novel devices used in different applications. IO devices use different materials for fabricating optical waveguides with current research employing different polymer materials with new research developments in polymer materials' improving their properties and features has made them very popular among researchers. The combined properties of polymer materials and optical waveguides have resulted into a new dimension of research for developing various devices from prototype designs to real-time applications of novel devices finding applications in all fields and areas. IO sensing is one of the areas that have gained a lot of momentum in recent years. Since, sensors are used for measuring and sensing physical, chemical, biological parameters suited for different applications and systems, an IO sensor proves to be a very efficient sensing device. Also, various fabrication and micro-fabrication techniques are employed to develop polymeric waveguides for different applications. Design and development of novel devices using an appropriate fabrication technology is an interesting area of research. The research involves design of polymeric waveguide devices and at the same time use of an appropriate micro-fabrication method for developing these novel devices suited for various applications.

Research and development on IO sensors is mainly driven by the prospect of arriving at cheap multi-purpose sensing systems which would enable us to measure in real time very small changes of physical or chemical parameters [1].

The current technique used to fabricate polymer waveguide devices, such as the interferometers, resonators, couplers etc., is based mainly on spin coating and photolithographic patterning [2]. With this technology, a photomask that defines the geometric patterns of the waveguide devices must be designed and fabricated first. The waveguide patterns are then transferred from the photomask to the photosensitive polymer-coated substrate by exposing it to the ultraviolet (UV) light. Two drawbacks associated with the conventional fabrication method are

- The cost to make the photomasks is high and
- New photomasks must be designed and fabricated for any design and design modifications, which increase product development cost and time.

These drawbacks prove to be one of the major bottlenecks in the photolithographic method. One possible solution to this dilemma is to develop a maskless technology for defining geometric patterns, thus increasing efficiency and reducing production cost.

Maskless patterning techniques, including electron-beam writing [3, 4], ion-beam direct writing[5], and laser direct writing (LDW) [6, 7, 8], are alternate polymer waveguide (core layer) fabrication approaches that eliminate all steps associated with the definition of structures using photolithographic techniques.

Compared to the first two maskless techniques, which require a highly vacuumed operating system, the LDW technique, which is operated in an environment, is convenient and less expensive. A single-mode polymer waveguide with the LDW for optical communications applications has been demonstrated [7]

To develop devices using maskless patterning techniques various optical waveguide designs are available like interferometers, resonators, modulators, coupling based devices etc. In the past, devices like Mach-Zehnder interferometer (MZI) [9]; ring resonators [10] have been popular for designing of IO devices for their respective advantages. Mostly, interferometric devices are preferred over other configurations because of its optimum performance on one hand and relatively simple to implement basic structure on the other in integrated optical systems. Interferometers provide the flexibility to be used in various applications like IO sensors, immunosensors [11], temperature variation devices etc. Interferometers provide a basic structure in integrated optics with a chemo-optical interface layer. Hence, MZI is one of the work-horses in the field of IO chemical sensors [10]. Hence, developing a MZI IO sensor using innovated fabrication technique can result into a highly efficient device. The MZI design and properties are discussed in detail in later chapters with different methodologies used to develop novel devices.

IO sensors can be implemented for chemical biological sensing applications [12, 13] by developing an array of sensors on a single system enabling sensing of multiple analytes simultaneously. Some of the advantages of

micro fabricated IO sensors include small device size and sampling volume, the possibility of batch processing, the optional co-integration of electronics, and the reproducibility of sensor characteristics due to precise geometric control in the fabrication steps [1]. These advantages in recent times have generated a huge demand for developing smaller biosensors and micro biosensors [14] for determination of mechanisms and kinetics of biological events. Developing an IO sensor array for such applications require innovative techniques other than photolithography and spin coating.

For general interferometer applications, the interferometers upper cladding layer can be spin-coated to cover both arms. However, when the interferometer is used as a sensor, its sensing arm and reference arm should be covered with different upper cladding materials. Within a sensor array, individual sensors need their own sensing pads for the simultaneous detection of multiple analytes. Therefore, spin coating can no longer be used for upper cladding fabrication. The current technique used to fabricate the upper cladding layer of a sensor is based on spin coating and etching or lift-off process followed by the sensing pad's deposition. The material used for the reference arm is first spin-coated; the coating covers both the sensing and the reference arms. The photolithographic technique is used to lift off the reference materials above the core layer of the sensing arm, and then the sensing material is deposited. The photomask is required for the lift-off process before sensing material is deposited. This makes the current technique of photolithography and spin coating unable to develop

sensor arrays and multiple sensor devices especially for prototype designers, individual researchers and small laboratories where making photomasks is not viable being a very expensive methodology. An alternate maskless technology is the need and one of such methodologies is fountain pen micro-patterning [15]. The innovative application of the fountain pen-based micropatterning technology to sensor array fabrication will allow simultaneous deposition of multiple waveguide sensing pads on the same layer, which can't be done by the conventional spin-coating method. The fountain pen-based micropatterning technology holds great promise for advanced polymer deposition, allowing different patterns (continued and discrete) to form on a variety of substrates. For a maskless chemical and biological sensor/sensor array fabrication system, the LDW technique will be used for waveguide fabrication and the fountain pen-based micropatterning for direct deposition of the sensing pad, thus providing an extremely simplified fabrication process.

1.2 Purpose and Objectives of the Study

This research lays the foundation for a highly simplified system for micro fabricating polymer-based sensor arrays that are compact, highly sensitive, and user-friendly. The purpose of the research is to develop a combination of a highly simplified maskless micro fabrication LDW technique and fountain pen based micro-patterning technique to fabricate and characterize the chemical/biological sensor/sensor array prototype using this simplified fabrication method.

The main objectives of the study are as follows:

- To fabricate the MZI core layer using the LDW to replace the multistep photolithography process

LDW is used to pattern the core layer material of the waveguide. The waveguide's core layer material is transparent at working wavelengths (e.g., 632 nm or 1550 nm) and has a strong absorption in the UV region. The core layer is selected considering the above criteria so that the material can be patterned by the LDW. The waveguide's width and thickness created by the LDW rely on the UV light power and its spot dwell time on the sample. With fixed UV power, different dwell times are tested to attain a MZI (a few microns in width and height typically less than 10 microns) on a silicon or glass substrate with a prefabricated lower cladding layer.

- To fabricate the upper cladding layer by using the fountain pen based micro-patterning system and spin coating method

  The upper cladding layer is coated using the spin coating process and using fountain pen based micro patterning system for comparison purposes. Both the sensing material and the reference material used for the upper cladding layer are tested first to make sure that they are easily formulate to printable polymer fluids that are suitable for precision printing. Different combinations of such parameters as the concentration of the solution, the pressure or vacuum applied to the nozzle, and the sample's moving speed relative to the print head that affect the pipette. Outcomes

are tried to achieve optimum printing results. The sensing pad's thickness above the core layer is of the order of few microns.

- Evaluate and compare the sensors

  The finished waveguide sensors are evaluated on the basis of their performance as general interferometers. The waveguide developed using the Fountain pen based micro patterning based system is compared with the waveguide developed using the spin coating method for coating of upper cladding of the waveguide. The resulting output power profile of the waveguides is generated to confirm their functionality as general interferometers.

1.3 Research Questions

The research question associated with this study are stated below for hypotheses testing,

Research Question: Can the combination of micro-fabrication technique of LDW and fountain pen based micro-patterning be used to develop the MZI for chemical/biological sensing applications with a minimum waveguide propagation loss?

- Null Hypotheses:

  Combination of micro-fabrication technique of LDW and fountain pen based micro-patterning can be used to develop the MZI for

chemical/biological sensing applications with a minimum waveguide propagation loss.

- Alternate Hypotheses:

  Combination of micro-fabrication technique of LDW and fountain pen based micro-patterning cannot be used to develop the MZI for chemical/biological sensing applications with minimum waveguide propagation loss.

1.4 Scope of the Study

The research is devoted to the novel use of LDW technology combined with fountain pen-based micro patterning technology for polymer-based MZI sensor fabrication. The sensor sensitivity for a chemical and biological sensor will not be tested. The general interferometer function of the sensors is being tested to prove the working of the MZI developed by using the simplified fabrication technique, The research provides methodology that focuses on mask less technology, allowing the definition and modification of geometric patterns through the programming of computer software, in contrast to the conventional mask based photolithographic approach, in which a photomask must be produced before the device is fabricated. The research lays the foundation of unique incorporation of the LDW and the fountain pen-based micro patterning fabrication process into the research and development of sensor arrays will lead to a much more practical and flexible prototype of a high-sensitivity sensor array. The

research can also serve as a step toward the development of a maskless manufacturing system of polymer IO devices, such as modulators, interferometers, couplers, and switches.

CHAPTER 2

REVIEW OF LITERATURE

2.1 Background

Sensor in the simplest form is defined as a device or a system used to measure a property or quantity and give a quantified output. The resultant output of the sensor and its usefulness is what makes the sensors so important in real life. Sensors have evolved tremendously from the bulky systems like thermisters to micro optical sensors ranging their sensitivity to all areas like acoustic, biological, chemical, electric, magnetic, optical, mechanical, radiation, thermal and other applications [16, 17]. Classification of such a huge set, which range in all areas and fields, becomes very difficult. One way of sensor classification is by looking at all of its properties such as what it measures (stimulus), what its specifications are, what physical phenomenon it is sensitive to, what conversion mechanism is employed, what material it is fabricated from, and what is its field of application. This type of classification is explained by Jacob Fraden [16] and such a broad range of classification considers all aspects of sensors and provides a good background to choose an appropriate sensor or classify a developed sensor. For example, Based on the above classification method a surface acoustic- wave oscillator accelerometer is classified as a sensor for stimulus acceleration with specifications sensitive in frequency shift per g of acceleration, short and long term stability in Hz per unit time, etc. having a

mechanical detection means and electrostatic conversion phenomenon of made of organic insulator applicable in automotive, marine, space and scientific measurement.

As the size of the sensor goes on decreasing, technology is going from a single sensor to multiple sensors on a single platform forming an array of sensors or a sensor array. A sensor array is defined as a set of sensors of the same type fabricated together on a single base or chip. With system's getting complex day by day such sensor arrays are becoming need of the hour for parallel emerging technologies. Also, with the availability of micro sensors and technology going towards nanometrics, sensor arrays are useful devices to combine a variety of stimuli measurement simultaneously on one single chip and developing a compact and more accurate system of sensors. Sensor arrays can be built on one single optical chip allowing it to be the heart of a multi-purpose sensing system. Optical methods play a significant role in this transformation, since optical methods scale the size of devices tremendously helping to achieve sensor networks and arrays alongwith a lot of advantages like being guided wave systems; the optical path is well defined excluding the necessity of (re-) adjustment of positions of the bulky components compared to other methods [10]. Optical systems' allow for simple guidance of light towards and from the optical chip enabling remote sensing and the construction of extended sensor networks. Optical methods are very popular today for their great sensitivity and large bandwidth along with developing compact, rigid and provide a great

flexibility in choosing materials and structures giving additional degrees freedom for effective optimizations and indeed IO chemical sensing detection limits are of the order of magnitude of some parts per billion (ppb)[10]. An IO biosensor can be classified as a device measuring optical stimulus having sensitivity in the refractive index change due to the analyte contact with IO detection using polymer materials for biochemical transformation with applications in health, chemical, medicine and biological areas.

Optical methods have proven to be reliable and successful in the last decade for developing quality sensors for different applications and successfully integrating them with electronics. Some of the devices developed include resonators [10], modulators [18], couplers, interferometers [7, 9], immunosensors [11], grating filters [2, 3] for different areas and applications like chemical sensing [10, 12, 19], biological sensing [9], telecommunications [20, 21] etc. Concentrating on IO biosensors, different design methodologies have been introduced to fabricate these devices over the period of time to achieve great sensitivity and efficiency for their respective purposes. Methodologies like photolithography, maskless techniques like electron-beam writing, which requires a vacuum environment, considering the fact that a building and maintaining a vacuum environment requires a lot of resources and energy which is not always viable [3, 10], proton-beam writing[20], ion-beam writing, a dry etching process implemented is a non – reactive ion etching process by means of a focused ion beam produced by an ionic column devoted to micro-machining in polymers [5]

and LDW, compared to other techniques is a much simpler and operated in a standard room is a very viable methodology for fabricating waveguiding devices for sensors and other devices[6, 7, 8]. With a strong background of efficiency and reliability of IO sensors in various applications research and technology moves in further strengthening and going in the direction of development of complex devices like arrays of multiple sensors.

The current sensor fabrication technologies are not directly applicable for developing complex devices like sensor arrays and need new methods for developing such sensors. Some prevailing technologies can be modified and used for the designing sensor arrays like photolithography is combined with the lift-off process to implant different material on the same base to create a multiple sensor array. Some of the works done in recent past and current technologies are discussed for fabricating novel sensor devices for high sensitivity, efficiency and cost effectiveness. Some of the research advances are techniques like Sol-gel immobilization method for fabricating an array based enzymatic optical biosensor [22], but having a disadvantage of inherent limitations like poor adhesion of sol-gel onto the solid structure and fragileness of the final structure associated with the shrinkage of the gel. A more standard technology used for developing biosensor arrays or microarrays is the Fluorescence detection for quantifying extents of hybridization between surface-immobilized probes and fluorophore-labeled analyte targets in DNA microarrays [23]. Another simplified methodology is the multiplexed electrochemical detection which requires an

electronically active substrate to analyze each array site and benefits from the addition of integrated electronic instrumentation to further reduce platform size and eliminate the electromagnetic interference that can result from bringing non-amplified signals off the chip. An active electrochemical biosensor array, constructed with a standard complementary metal-oxide-semiconductor (CMOS) technology, to perform quantitative DNA hybridization detection on chip using targets conjugated with ferrocene redox labels has been demonstrated [23]. Research has been done for developing optical and fluidics systems as central components for an automated array biosensor. Disposable planar waveguides are patterned with immobilized capture antibodies using a physically isolated patterning (PIP) method. The PIP method enables simultaneous deposition of several antibodies and completely circumvents cross-immobilization problems encountered with other array deposition processes [24]. Also, a novel and sensitive multi-through put localized surface Plasmon resonance (MSLPR) biosensor was developed for the first time. Various gold nanorods with different aspect ratios were used to fabricate the optical sensor. The MLSPR based optical biosensor can be used to detect three antigen-antibody pairs simultaneously labeling procedure not necessary [25]. One more area of research for developing sensor arrays is Electro-static self assembly (ESA) method used for developing sensor transducers to detect volatile organic compounds [26]. Some of the sensors developed using these technologies are optical biosensor array based on natural ion channels[27], PDMS microdevice

with built in optical biosensor array for on-site monitoring of the microenvironment within microchannels[28], liquid core optical ring resonator label-free biosensor array for lab-on-a-chip development[29], initial demonstration of a local, evanescent, array coupled biosensor concept[30], local evanescent, array coupled (LEAC) biosensor response to low index adlayers[31], etc. Another direction where prominent research is going on is using a particular method called fountain pen lithography to deposit arrays of molecularly imprinted polymer on the fabricated waveguide which is combined with sensor fabrication techniques to develop sensors for various applications [32]. It uses theory of evanescence for detecting change in the refractive index induced form the analyte contact. This technique has a strong potential for the fabrication of microchips and other types of integrated optical chemical and biosensors because of its simple and efficient methodology [32]. Such a technique easily combines with currently existing techniques to form an innovative microfabrication technique for developing IO sensor arrays containing configurations like resonators, couplers, and interferometers etc. for chemical/biological sensing applications the evanescent wave theory [19] principle used fountain pen lithography is explained briefly for further understanding the behavior of an IO biosensor developed using this technique.

2.2 Evanescent Wave Theory

The Evanescent theory explains the principle of sensitivity of an optical waveguide as follows, light traveling in a waveguide is confined within a core sandwiched between cladding layers with lower indexes of refraction. Total internal reflection occurs if the angle θ (Figure 1) of the internal incident light is greater than the critical angle. The critical angle is defined as $\theta c = \sin^{-1}(n_2/n_1)$, where n_1 and n_2 are the index of refraction of the core and the cladding, respectively. Although the light energies are totally reflected, the electromagnetic fields, known as evanescent wave [33], still extend beyond the interface and into the cladding. The penetration depth depends on the internal incident angle, which is sequentially related to n1 and n2. The evanescent field can be expressed as,

$$E = E_0 \exp(-x/d_p) \quad \ldots\ldots (1)$$

Where, E_0 is the field amplitude at the boundary, d_p is the penetration depth given by,

$$d_p = \frac{\lambda}{2\pi n_1 \sqrt{\sin^2\theta - (n_2/n_1)^2}} \quad \ldots\ldots (2)$$

The penetration causes the reflected light to shift laterally relative to the incident light at the boundary, which is known as Goos-Hanchen shift shown in Figure1, and at the same time it produces a phase shift between the incident and the reflected light. The phase changes for the transverse electric field (TE), $\Delta\phi_{TE}$, and for the transverse magnetic field (TM), $\Delta\phi_{TM}$, can be expressed as,

$$\Delta\phi_{TE} = 2\tan^{-1}(\sqrt{\sin^2\theta - n_2^2/n_1^2} \;/\; \cos\theta) \quad \text{..... (3)}$$

$$\Delta\phi_{TM} = -\pi + 2\tan^{-1}\left(\sqrt{\sin^2\theta - n_2^2/n_1^2} \;/\; ((n_2^2/n_1^2)\cos\theta)\right) \quad \text{..... (4)}$$

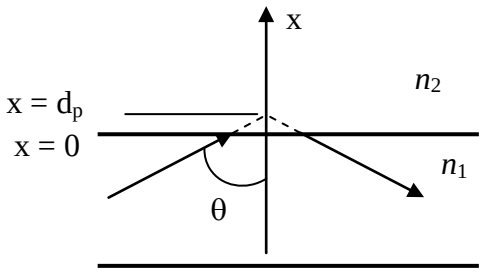

Figure 1: Goos-hanchen shift for evanescent wave [33].

According to equation (1), the evanescent field is inversely proportional to the distance from the boundary (x = 0). Penetration depth based on equation (2) is only a few wavelengths (for example, given n_1=1.461, n_2=1.457, and θ=88^o, the penetration depth is about 1.7λ). Based on equations (3) and (4), changing the cladding index of refraction, n_2, will give rise to a phase change in the evanescent light. This change can be easily detected as a light intensity change. This principle is used in IO sensors and sensor arrays for sensing and characterizing optical waveguide devices like interferometers, couplers, modulators etc. waveguides are an integral part of an IO sensor and choosing a particular design of waveguide device is very important. Waveguides with polymer materials are used to develop devices like interferometers, resonators with the stimulus being placed over the cladding layer of a device which interferes and brings a change in the refractive index of the polymer which is

measured using the evanescent wave principle. There are many polymer waveguide devices and we choose a specific design for a specific application like a chemical/biological sensor.

Polymer waveguides are classified as active and passive waveguides; some of them are listed below,

a) Passive waveguide devices: Coupler/splitter, Grating/filter, delay line, mode converter, attenuator, Array waveguide (AWG).

b) Active waveguide devices: light emitters, laser, light detectors, optical modulator/switch, accelerometer, interferometer, chemical detector.

Interferometers are hugely preferred because of their simple design which allows its easy implementation into different applications. They provide a basic structure in integrated optics with a chemo-optical interface layer. MZI has been tremendously used by researchers for developing various devices considering its advantages. Some of the research where MZI [7] has been implemented are switching & modulating purposes, optical interconnect applications, telecommunications, chemical sensing, biosensor applications etc. Hence, combing the properties of polymer materials with the advantages of an MZI used in a multiple sensor technology to develop a chemical/biological sensor/sensor array with a simplified micro fabrication technology will yield a very effective, efficient, simple and a useful device.

2.3 Polymer MZI as a Chemical/Biological Sensor

Polymer MZIs with chemical/biological-selective materials in one arm have been shown to be extremely sensitive to chemical and biological analytes in both vapor and liquid formats [34]. MZIs, therefore, hold great promise for accurately identifying and detecting a variety of chemical and biological particles in the air or on surfaces. To realize the full potential of the MZI sensor technology, arrays of individually functionalized MZIs are required for simultaneous detection of multiple particles.

A polymer MZI is a two arm multilayered optical integrated waveguide structure with a core layer (less than 10 micrometers in width and height) surrounded by upper and lower cladding layers. For sensor purposes, one MZI arm is used as the reference arm and the other arm is the sensing arm, with a portion of the upper cladding used as sensing pad. The schematic of a single MZI sensor is depicted in Figure 2. The operating principle of an MZI can be described as follows: The incident light coupled into the waveguide's core layer is split equally between the two arms of the MZI. The two split lights recombine at the output. The output light intensity depends on the relative phase of the recombined lights. In other words, the relative phase of the recombined lights can be detected by measuring the output light intensity.

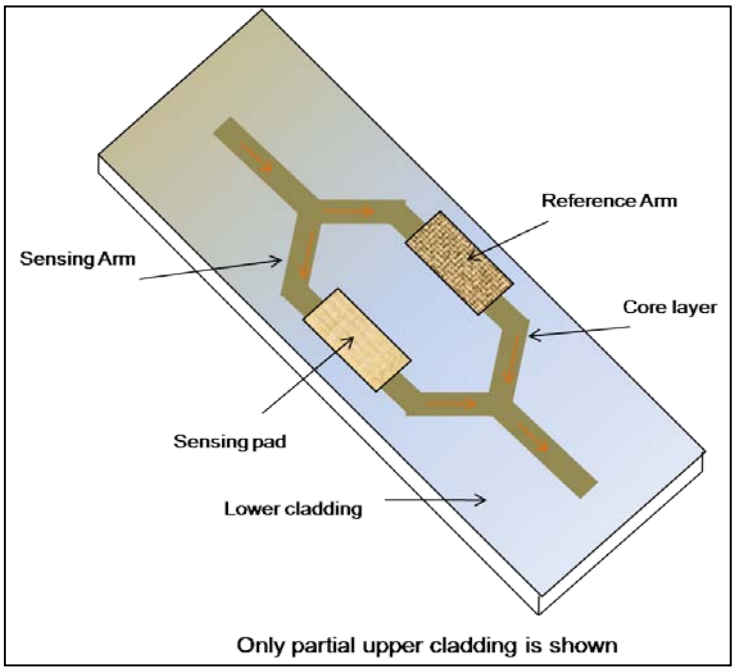

Figure 2: MZI, a chemical/biological sensor.

The interaction between the sensing pad (consisting of the receptor, which is specific for the particles of interest) and the targeted particles (such as vapors from explosives, metal ions, or bacteria) that attaches to the receptor alters the light phase in the sensing arm relative to that in the reference arm. Therefore, the light intensity measured at the output of the device is a function of the amount of "attached analyte" bound to the waveguide's sensing pad.

CHAPTER 3

RESEARCH METHODOLOGY

3.1 Polymer Materials for Fabrication

Before the fabrication process, a brief summary of the materials used in the fabrication of the core layer and the cladding layer of the MZI biosensor is explained. The lower cladding is a Silicon oxide layer fabricated over the silicon substrate is used. SU-8 photoresist is used as the core layer and the NOA 61 is used as the upper cladding of the fabricated biosensor.

3.1.1 SU-8 photoresist as the core layer

SU-8 is a high contrast, epoxy based photoresist designed for micromachining and other microelectronic applications, where a thick, chemically and a thermally stable image is desired. SU-8 has been tested by many researchers for developing and designing different polymeric optical devices using different fabrication methods [20] and used in many applications like embedded micro channeling [21], IO sensors [19], etc. SU-8 exhibits low optical losses at infrared wavelengths making it very important for developing polymeric waveguides and microsensors [35]. Figure 3 explains the relation between the thicknesses of the SU-8 thin film with respect to the spin speed used for coating of the SU-8 film. SU-8 2005 is used for experimentation in the laboratory for fabricating MZI for chemical/biological applications. From Figure 3, it is evident that a thin film of thickness of 5 microns can be spin coated at spin speeds of

3000 to 4000 rpm. The exact procedure used for fabricating the SU-8 thin film is explained in section 3.4.

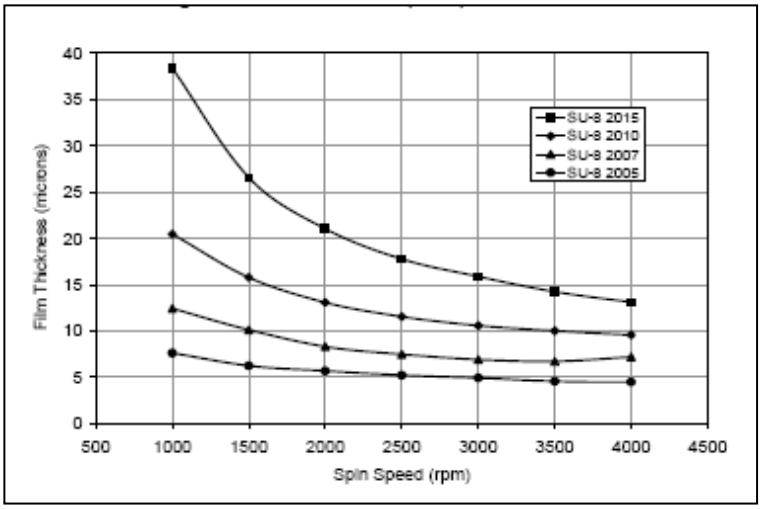

Figure 3: Spin speed vs. thickness for SU-8 [36].

SU-8 2005 has excellent imaging characteristics and is capable of producing very high aspect ratio structures. Use of a faster drying, more polar solvent system results in improved coating quality and increases process throughput. Film thickness of 0.5 to >200 microns can be achieved with a single coat process. The exposed and subsequently thermally cross-linked portions of the film are rendered insoluble to liquid developers. SU-8 2005 is best suited for permanent applications where it is imaged, cured and left on the device [36]. The characteristics and features are ideal for the use of LDW and developing devices like the MZI. Following explains the step-wise sensor fabrication process using the SU-8 polymer.

3.1.2 NOA 61, upper cladding

Norland Optical Adhesive 61 (NOA 61) is a clear, colorless, liquid photopolymer that will cure when exposed to ultraviolet light. Since it is a one part system and 100% solids, it offers many advantages in bonding where the adhesive can be exposed to UV light. a) The use of NOA 61 eliminates premixing, drying or heat curing operations common to other adhesive systems. b) Curing time is remarkably fast, and is dependent upon the thickness applied and the amount of ultraviolet light energy available. c) The adhesive is designed to give the best possible optical bond to glass surfaces, metals, fiberglass and glass filled plastics. d) NOA 61 also has excellent clarity, low shrinkage and as light flexibility that make it superior to other materials for optical bonding. These characteristics are important in order for the user to produce high quality optics and achieve long term performance under changing environments [37]. The Figure 4 gives the relation of refractive index with respect to wavelength and Figure 5 shows the index variation of NOA 61 across room temperature. The refractive of the cured NOA 61 film is 1.56. The Figure 4 and 5 help to calculate the optimum index difference between the core layer and cladding layer. The thickness of the upper cladding layer need not to be specific and a considerable layer with more than 2 microns thickness provide acceptable results.

NOA 61 is cured by ultraviolet light with maximum absorption within the range of 320-380 nanometers with peak sensitivity around 365nm. The recommended energy required for full cure is 3 Joules/sq. cm in these

wavelengths. The cure is not inhibited by oxygen; hence any areas in contact with air will cure to a non-tacky state when exposed to ultraviolet light.

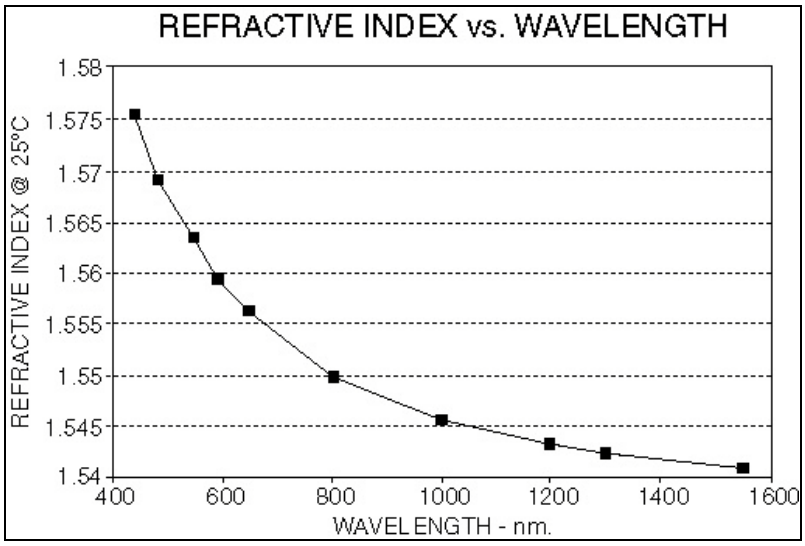

Figure 4: NOA 61 refractive index distribution over wavelength [37].

In most optical applications, curing is done in two steps. A short, uniform exposure, or precure, is used first. The precure time is of sufficient duration to set the bond and allow it to be moved without disturbing alignment. This is followed by a longer cure under UV light to obtain full cross linking and solvent resistance of the adhesive. The precure can be obtained in 10 seconds using a 100 watt mercury lamp at 6".Where longer time is required for alignment; it can be extended to a few minutes using a very low intensity light source. The final cure can be accomplished in 5 to 10 minutes using the 100 watt mercury lamp. The precure allows the user to align and set the precision parts quickly and minimizes the number of holding fixtures required.

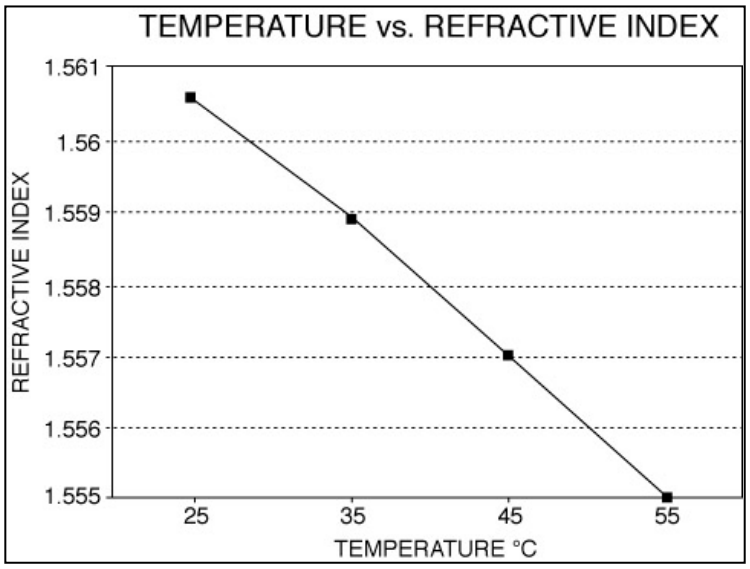

Figure 5: NOA 61 refractive index distribution over temperature [37].

After the precure, excess adhesive can be wiped up with an alcohol or acetone moistened cloth. Assemblies should be inspected at this time and rejects separated in methylene chloride. The bonded area must be soaked in the solvent and normally will separate overnight. The time required to break the bond depends upon the extent of the cure and the size of the bond area. When fully cured, NOA 61 has very good adhesion and solvent resistance. NOA 61 can withstand temperatures before aging from -150° C to 125° C.

3.2 Design of a Chemical/Biological MZI Sensor.

The MZI is designed in RsoftCAD software before the actual fabrication to know the behavior of the device and determine its physical parameters for fabrication. A MZI with a core less than 10 microns (height and width) on a silicon substrate with silicon oxide as the lower cladding and NOA 61 as the upper

cladding are designed using the RSoft CAD tool [38] and is tested in simulation software called BeamPROP [39]. The designed MZI is shown in the Figure 6.

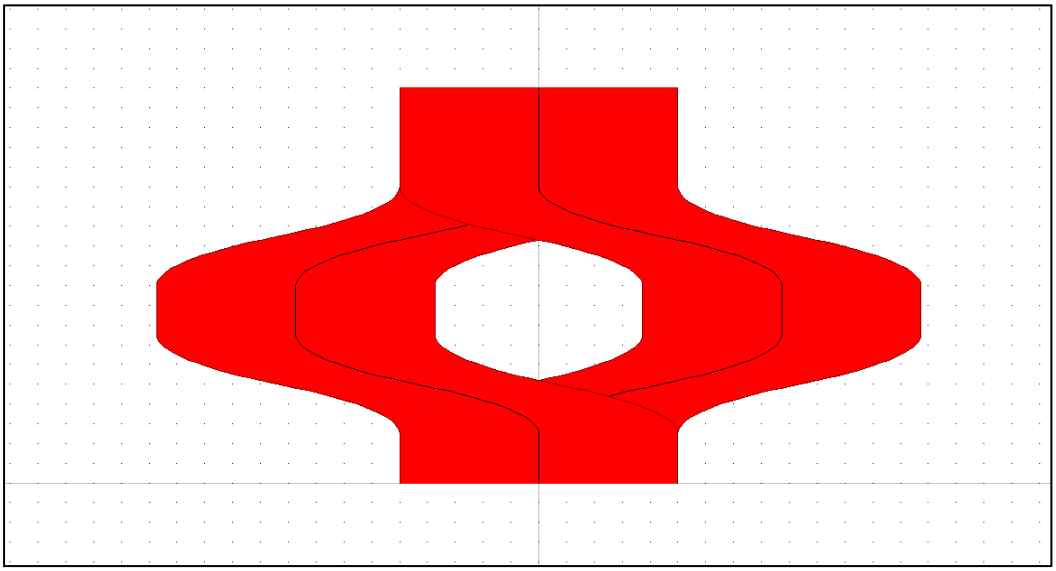

Figure 6: MZI schematic in Rsoft CAD.

The designed MZI is a 3D rib channel waveguide subjected to a wavelength of 1550 nm. The height and width considered for the simulation are 5 microns. The lower cladding is silicon oxide layer with a refractive index of 1.46 on the silicon substrate. The core layer is an active polymer SU -8 with a refractive index of 1.59 calculated using the prism coupler [40]. The upper cladding is developed using NOA 61 with a refractive index of 1.56. The designed MZI being a 3D rib channel waveguide, for which, the integration area depends upon the type of waveguide structure, the program will integrate over a rectangle with width and height determined by the waveguide parameters. The monitors also have a shape depending on the structure and for the designed MZI

it will choose the rectangular shape. This is seen in Figure 7, which gives the index profile of the designed waveguide. The index profile is used to confirm the design of the MZI in terms of dimensions, wavelengths and refractive indices of the core and cladding layers. The X axis gives the width of the waveguide in microns and Y axis gives the height in microns. The scale on the right gives the refractive index distribution of the waveguide showing the red rectangular area as the core layer with the yellow upper cladding and the purple lower cladding.

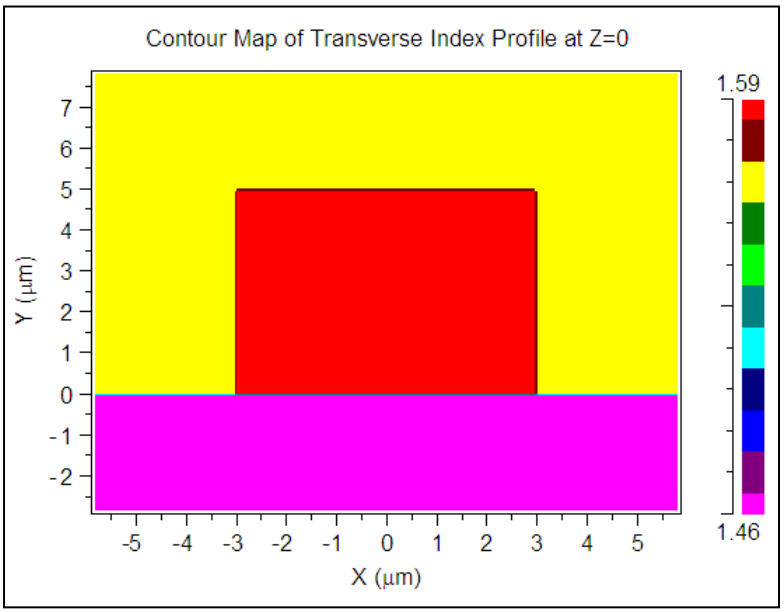

Figure 7: Index profile of SU-8 waveguide in Rsoft CAD.

The designed MZI is scanned across the width and height for calculating the number of modes to obtain the number of modes using the mode calculation utility in BeamPROP. Figure 8 gives the graph generated showing the different modes existing at different widths for the designed waveguide. The MZI is

scanned with the height being constant and modes are calculated across the width of the waveguide. The graph shows the trend that more number of modes exists at higher widths.

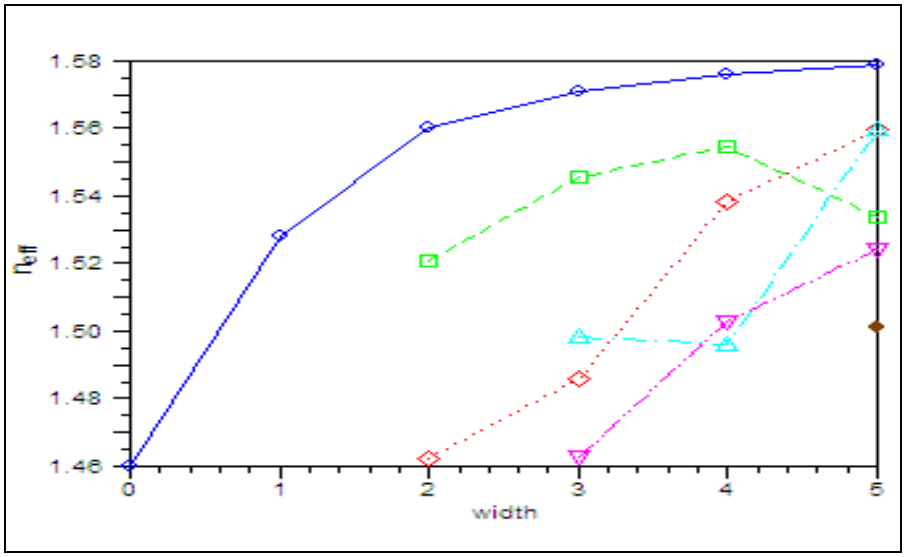

Figure 8: Mode calculation using BeamPROP simulation

The BeamPROP is a very efficient tool providing adequate tools to design and compute waveguides and other optical devices. The BeamPROP is used to provide a general simulation package for computing the propagation of light waves in arbitrary waveguide geometries. The computational core of the program is based on a finite difference beam propagation method (BPM) [39].

BPM is the most widely used propagation technique for modeling integrated and fiber optic photonic devices and most commercial software for such modeling is based on it. Some of the significant reasons for the popularity of BPM are as follows,

• BPM is conceptually straightforward, allowing rapid implementation of the basic technique. This conceptual simplicity also benefits the user of a BPM-based modeling tool as well as the implementer, since an understanding of the results and proper usage of the tool can be readily grasped by a non-expert in numerical methods.

• BPM is a very efficient method and has the characteristic that its computational complexity can, in most cases, be optimal, that is to say that the computational effort is directly proportional to the number of grid points used in the numerical simulation.

• Another characteristic of BPM is that the approach is readily applied to complex geometries without having to develop specialized versions of the method.

• The approach automatically includes the effects of both guided and radiating fields as well as mode coupling and conversion.

• Finally, BPM technique is very flexible and extensible, allowing inclusion of most effects of interest (e.g. polarization, nonlinearities) by extension of the basic method that fit within the same overall framework.

The designed MZI is simulated in BeamPROP with Gaussian power being applied at the input and its path is monitored and compared across the length in its two arms at 1550 nm wavelength. The power through the MZI and its path can be seen using the BeamPROP simulation tool. The Figure 9 monitors the path of the power through the waveguide when it is excited with a Gaussian launch power of 1550nm wavelength and with the dimensions same as that of the actual

waveguide to designed. The Figure 9 explains the travel path and its power levels across the length of the waveguide. From Figure 9 the waveguide is launched with Gaussian power and it travels through its length with the power splitting between the two arms and recombining in the output arm. This confirms the principle working of the MZI.

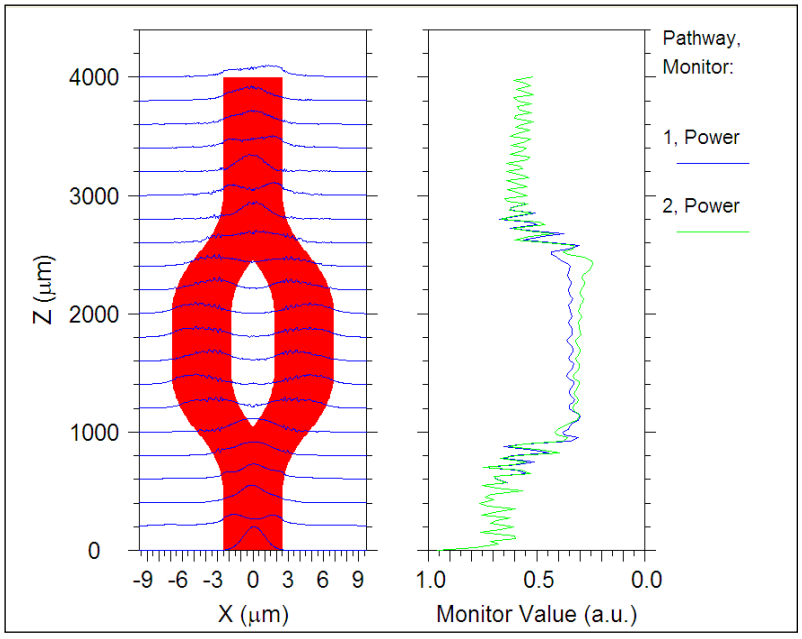

Figure 9: Waveguide power profile across the length of the MZI.

The Waveguide power (WG) is computed which is the integral power in the calculated field at the current Z position over the waveguide cross section. The integral is computed between +/- (w/2 + f/γ), where w is the waveguide width, γ is a characteristic transverse decay constant for the waveguide, and f is a fractional parameter set by the internal variable “monitor_decay_fraction” which defaults to 0. The characteristic decay length is determined from the highest

supported slab waveguide mode, but is appropriately limited if that mode is nearly cutoff.

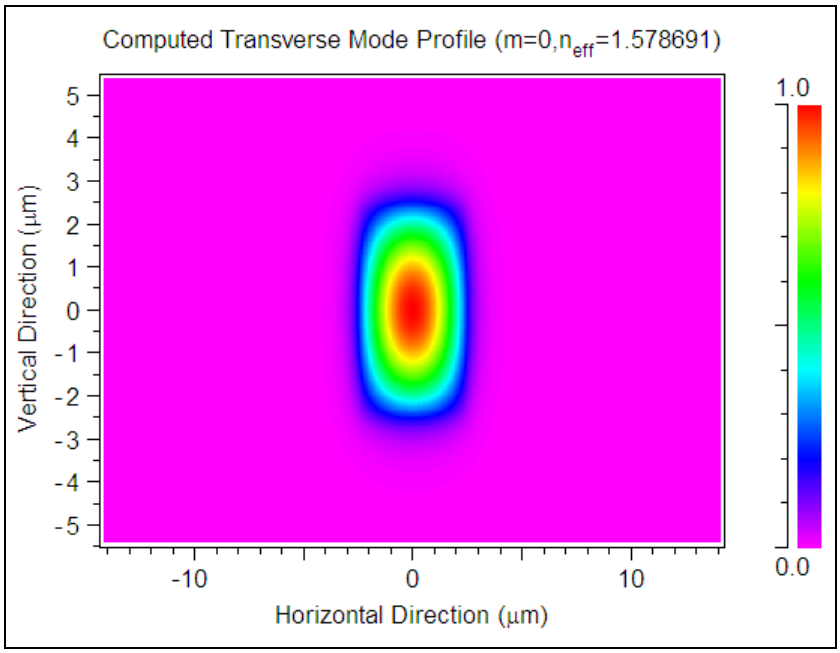

Figure 10: Different mode calculations in BeamPROP for SU-8 waveguide.

The simulation of the designed waveguide gives the actual modes in the waveguide; Figure 10 shows the fundamental mode. As the width and the height increases, more number of modes is seen in the waveguide. The fundamental mode shown is a transverse mode profile with maximum power being transmitted through the center. The center represents the core with the highest power carrying capacity through which the Gaussian power is launched. The Figure 10 shows the difference in the change of the index profile the Gaussian launch power. The radiation into the cladding can be seen. This radiation increases as we go to higher modes. The power loss is known based on the radiation and is minimal as most of the light couples in the waveguide core.

The design of MZI in BeamPROP simulation tool explains the behavior of the waveguide and a guideline for the expected results with the actual fabrication of the waveguide. The fabrication process of a chemical/biological MZI sensor is explained in detail in the further sections.

3.3 MZI Sensor Fabrication

The MZI sensor fabrication procedure is depicted in Figure 11. The silicon substrate is pre fabricated with a 2 microns thick cladding layer of silicon oxide. In step (a); the substrate is cleaned with great care to enhance the adhesion of the film to the substrate and the uniformity of the film.

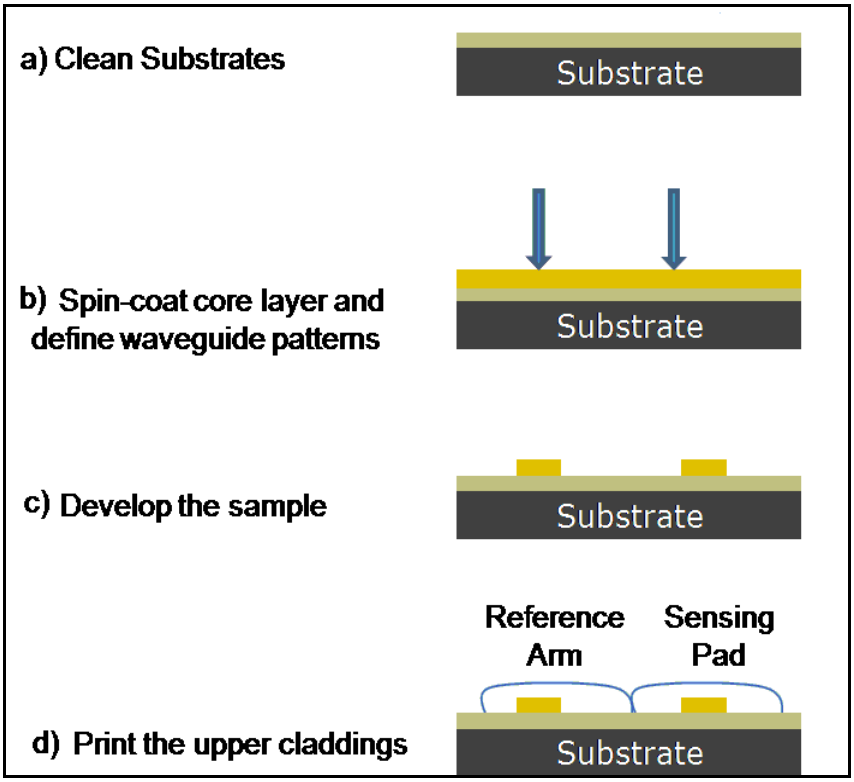

Figure 11: Sensor fabrication process.

In step (b), the core polymer thin film is spin coated, and waveguide patterns are defined with LDW by tracing the focused laser beam on the polymer's surface. After the sample is developed in step (c), the waveguides are formed. In step (d), A Fountain pen based micro-patterning is used to print the sensing material on top of the sensing arm's core layer, and the rest of the upper cladding is printed with the reference material. The spin coating methodology, LDW and fountain pen micro patterning is explained in detail in the following sections.

3.4 Spin Coating Methodology

The spin coating process is an important step for making of your sample; it controls the thickness of the thin film you make. The waveguide height is designed using the spin coating process. The thickness of the film is controlled by programming the spin speed and ramping speed and the duration of the photoresist spinner. A general guideline is provided by the manufacturer of the material/polymer regarding the thickness of the thin film on different substrates for different spin speeds. The correct thickness of the thin films is obtained by trying several different spin speeds, ramping speeds and different time durations. Also, with the right thickness the developed thin film should be nice and smooth, very uniform and clear to use it further in the design of the device development. A good thin film is obtained after thorough experimentation and running a

developed program with a combination of proper spin speed, ramping speed and their timing durations.

In general, the following spin coating trends are observed for most of the polymers,

- Higher spin speeds and ramping speeds result in thinner films.
- Spin speed and ramping speed have minor effects on the uniformity of the film.
- Solvents are mixed along with materials to make thinner thin films, but not necessarily smoother and more uniform films.

The PWM32 Photoresist Spinner (Headway Research, Inc.) is used for preparing thin films. The thin film is coated at various spin speeds and ramping speeds. These parameters and steps are programmed into available recipes of spin coating setup before spinning the thin films.

The following steps are used to prepare the thin films.

- Place a clean glass slide or substrate on the vacuum chalk.
- Select a particular recipe programmed for spin coating.
- Apply the solution on the glass substrate.
- Start the spin coating.

To create a recipe for spin coating following steps are used,

- Select a particular Recipe.
- Select step 1.
- Enter the required Spin Speed.

- Enter the required Ramping speed.
- Enter the desired Spin time.
- Enter the Termination Time (Spin Time).
- End the Recipe

Once a polymer waveguide is spin coated and the required thickness is obtained it is further taken for curing and then is fabricated for developing the exact width of waveguide.

Figure 12: Spin coating set-up in laboratory.

The program used for spin coating the SU-8 polymer as the core is as follows,

- Dispense 1ml of resist for each inch (25mm) of substrate diameter.
- Spin at 500 rpm for 10 seconds with an acceleration of 100rpm/sec
- Spin at 4000 rpm for 30 seconds with an acceleration of 300rpm/sec

The waveguide is designed using LDW which is briefly explained in the following procedures.

3.5 Micro-Patterning the Core Layer using LDW

The fabrication system consists of an XY precision stage capable of operating at mechanical resolutions of 10nm and repeatabilities of +-100nm, providing adequate precision for single-mode waveguide fabrication. To fabricate a waveguide, the laser sensitive polymer is spin-coated on a substrate. Waveguide patterns are written by tracing a laser beam through objective lens, which control beam size and consequently the waveguide's size across the surface of the polymer film. The film is then developed to remove the unexposed area. The actual set-up used in the laboratory for developing the SU-8 polymer waveguide is given in Figure 14. A fully automated LDW polymer waveguide fabrication system is depicted in Figure 13.

The output results from the above procedure yields good quality devices. The process requires little mechanism and labor for designing the whole process. LDW provides flexibility in focusing and controlling the incident energy levels. It also allows us to control the scanning speed for the fabrication of novel structures without affecting the surrounding environment. Thus, LDW is extremely useful for rapid and inexpensive prototyping.

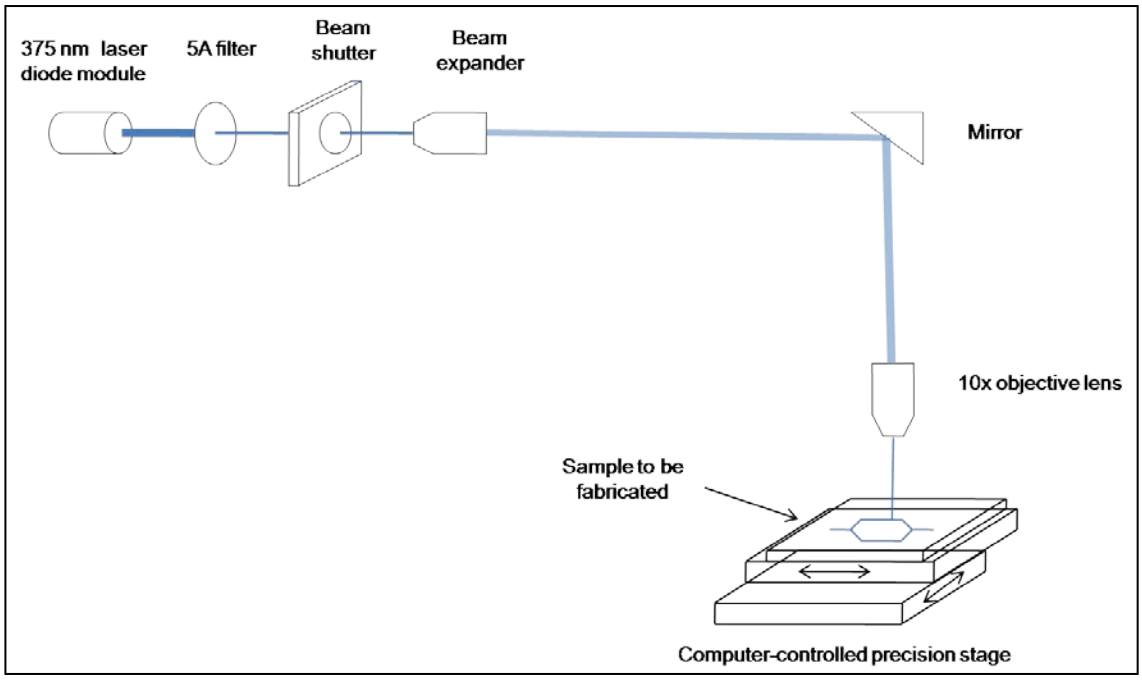

Figure 13: Laser direct writing system.

The intensity required to write waveguides on silicon oxide substrates using SU-8 200 as core is 100-110 mJ/cm^2. A matrix experiment is performed to determine the exact optimum dosage required. A visible latent image is seen on the thin film after 5-15 seconds after placing on the post exposure hotplate. The procedures required to follow for developing a waveguide is described as follows,

LDW patterning requires alignment of the laser to focus on the surface of the precision stage with maximum intensity and minimum area so that the complete laser power is focused on a needle tip point on the precision stage where the silicon oxide substrate with SU-8 is placed for micropatterning. The Figure 11 explains that in the LDW setup the laser has to pass through a filter, shutter, and beam expander directed through a mirror onto to an objective lens

which focuses the light on the precision stage. All these components have to be adjusted and aligned along with the laser for focusing the laser. The power of the laser can be manipulated using the filters of different intensities ranging from 1A to 30A. The height of the objective lens is adjusted to have the precise focusing of the laser. The beam expander and the mirror are aligned to retain the complete shape of the laser and direct it to the objective lens. Fine tuning of the laser is done after doing several experiments and fine adjustment of the height and position of the objective lens to get the right focusing, since, the focused beam point is in the order of microns it is not visible through naked eye and alignment through experiments is the only way to get the correct alignment by eliminating the error in each components one by one step wise and get the final correct alignment. After the alignment is finalized the waveguide design, in our case the MZI has to be designed in a G code program for a CNC machine (UNIDEX 600 series) [41] and run in a LabView environment which controls the precision stage. The precision stage moves below the laser focusing point according to our design and the design is micropatterned on the substrate with the spin coated material, SU-8. The program directs the precision stage to the position below the laser focus point and moves the stage to pattern the design with the exact required dimensions. The G code program [Appendix A] for a straight waveguide is written and tested below the laser for accuracy and after removal of errors actual experiments are done to get the desired width of the waveguide. Some amount of tuning is also required after this step to get ensure

the laser focusing is accurate, which is possible only after running few experiments and fine tuning through judgment. The focusing is very important because this decides not only the dimensions of the waveguide but also the quality of the waveguide. Once the focusing of laser and the G program are accurate the experiments are begun to fabricate the waveguide to get the desired width of less than 10 microns for the waveguide. The width is measured using the electron microscope in the laboratory. The steps of performing a particular experiment to fabricate are described in the Figure 11. Multiple runs of these steps are done till we get the desired results.

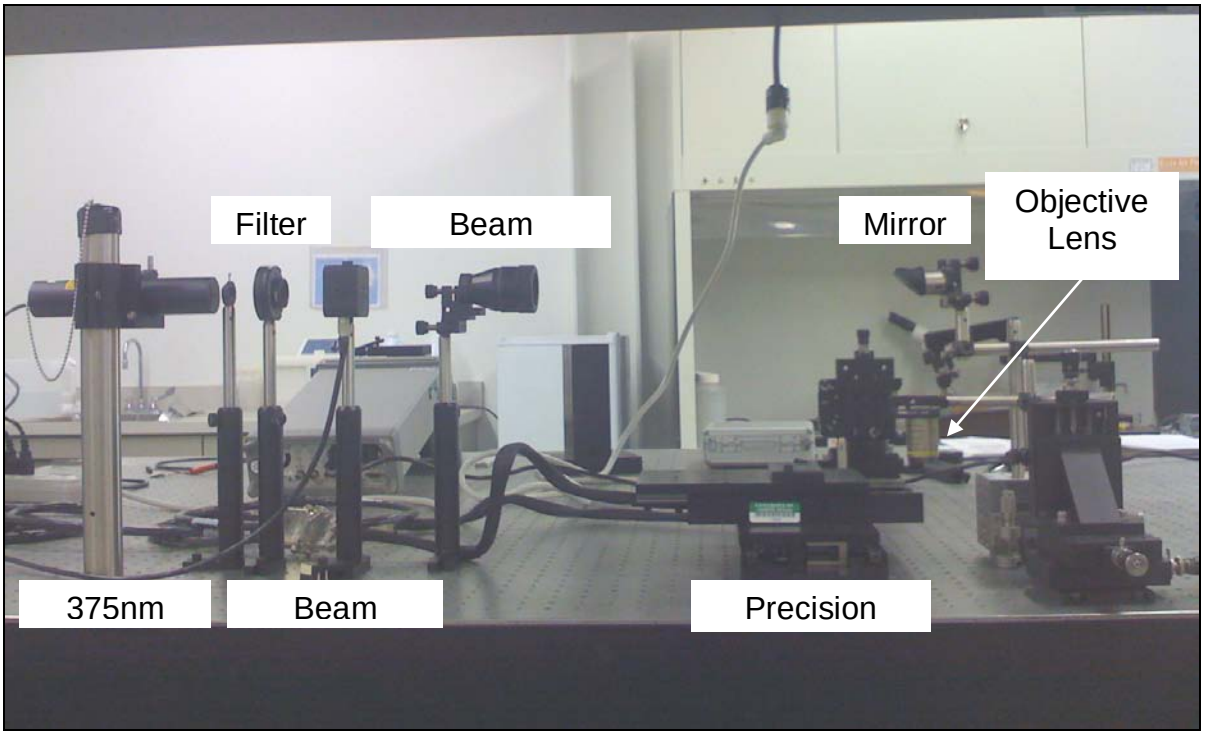

Figure 14: Picture of LDW set-up in the laboratory.

The experiment is started with the minimum filter 1A and with minimum speed of 1mm/sec. the speed is of the precision stage and is controlled in the G

code program. The filter is increased upto 5A and the speed in increased upto 5mm/sec. The above filter 5A the quality of the developed waveguide depreciates and hence, 5A filter is fixed and same is true for the speed above 5mm/sec. the width of the waveguide is still above 10 microns. The focusing of the waveguide is adjusted minutely at this stage to get a better waveguide and is done in clockwise and anticlockwise directions to get the best focusing. After an improvement in the width of the waveguide, the filter is increased to 6A since; we have slightly a better focusing laser point on the waveguide. Also, doing this gets the width below 10 microns and increasing the speed further gives a waveguide with 5 microns dimension of very good quality. This experiment is run multiple times with a silicon oxide layer as the substrate to confirm the result.

3.6 Fountain Pen Micro Patterning

The fountain pen principle associated with a small-scale pipette system shown in Figure 15 is available at the laboratory of small-scale instrumentation at the MEE dept. of UNT. The fountain pen has a position accuracy of +/-3um, an XY encoder resolution of 0.1 um, providing sufficient accuracy for the deposition of the upper cladding layer, including both sensing pads and the rest of the upper cladding layer. The fountain pen-based micropatterning provides an unparalleled advantage to the proposed sensor array fabrication by depositing different sensing materials on the same layer for multiple-sensing integration. The Figure15 shows a fountain pen micropatterning laboratory set-up.

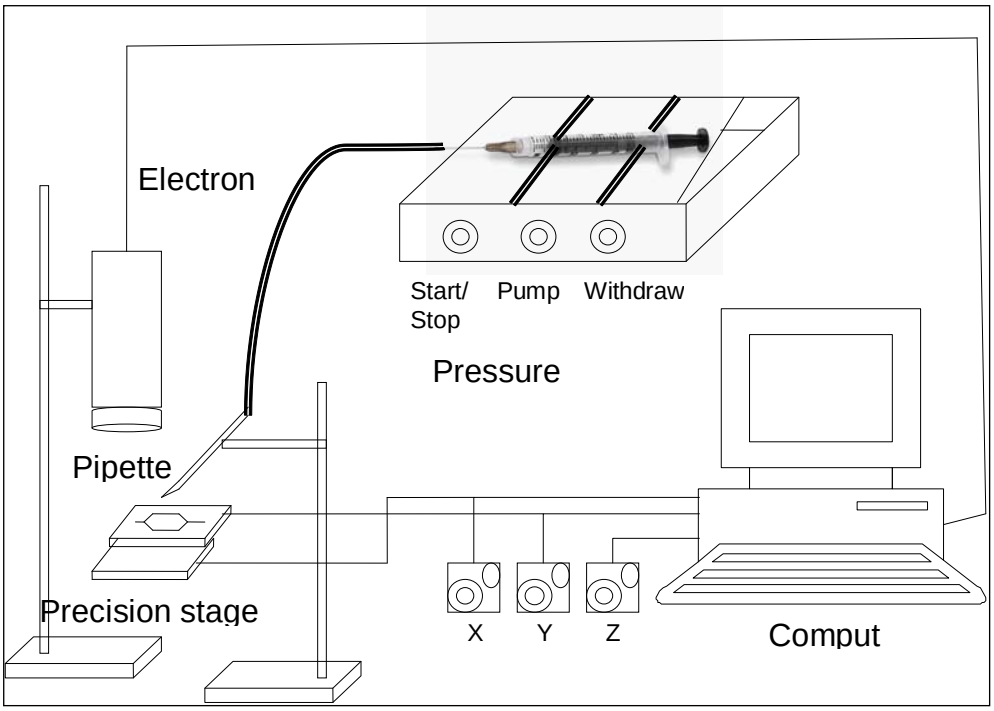

Figure 15: Fountain pen micro-patterning system.

The system above below comprises of a pipette used to pattern the polymer on the sample. A pressure controller is used to pump in the polymer from the pipette and to suck the liquid into the pipette. The pipette is initially grinded to get a suitable opening to drop the polymer onto the sample. The sample in placed on an XY precision stage which is controlled by the computer for moving in X and Y directions. The movement of the pipette is controlled in the Z direction. An electron microscope is used to control and precisely adjust the pipette on each waveguide. With the help of the computer and electron microscope a very precise adjustment is made and sample below in move in the X-Y direction. The Figure 15 shows the actual laboratory setup of the fountain open micropatterning system.

The fountain pen micro-patterning requires a very high level of precision and skill to handle the components and the pipette to pattern the upper cladding over the waveguide. The pipette is very delicate and its radius is of the order of nanoseconds which are used for dropping the cladding material onto the sample. Fountain micro-patterning involves 4 steps for performing the experiments, grind the fountain pen, fill the pipette with cladding material, align the sample with the pipette and perform the experiment.

Since, the diameter of the fountain pen is less than 1 micron and the waveguide fabricated is around 5 microns of width, the tip of the fountain pen has to be grinded to increase the diameter. To grind the pipette a current controlled rotary table is used powered by a voltage power supply. The surface of the rotary table consists of the sand paper allowing smooth grinding of the pipette. The pipette after coming in contact with the rotating table gets cut in the shape and the diameter of the tip of the pipette increases, at the same time it is connected to a pressure controller and it is pumping air continuously so that no particle gets stuck inside the pipette while grinding. The pipette is very delicate and care has to be taken to not push it and just touch it with light pressure on the rotary table giving enough contact for the grinding of the pipette. Such a precision is not possible through naked eye and the whole process is overseen from a very high resolution electron microscope interfaced with a computer and the pipette is focused and defocused cautiously while bringing it in contact with the rotary table. Throughout the grinding process the pipette is cautiously observed through

the microscope and carefully and slowly the pipette is grinded, this requires a lot of practice and skill to be developed to use the microscope and control the pipette. The pipette is then brought into contact with the cladding material NOA61 to be patterned on the waveguide. The pressure controller takes the pressure out of pipette to suck the cladding material and pressure is maintained to hold the cladding material inside the pipette.

After the grinding is done the pipette is taken over a translational stage where the sample is placed. The translational stage can be moved in X and Y directions controlled electronically through computer software from thorlabs inc. the pipette can be moved in the Z direction that is its height can be controlled. The whole alignment of the system is done under the observation of an electron microscope through the computer. Considering the delicacy of the pipette and freedom of few microns such an alignment requires a lot of skill with time and consistency to properly adjust the pipette over the sample waveguide on the translational stage. The pipette is aligned with the sample in X & Y directions by focusing the microscope on the pipette and then focusing it as the height is lowered on the sample to just keep in touch with the sample. This is done many times to get the correct alignment. Also the angle across the length of the sample is adjusted to keep it in a single plane; the height of the sample with respect to the pipette plays an important role since the pipette is of the danger of breaking if an angle exists or the waveguide is bound to get damaged. Also, for a smooth cladding layer over the waveguide the sample has to be adjusted very precisely.

Every minute adjustment has to be done through the microscope making it very complicated system.

Once, the alignment is done with pipette filled with the cladding material aligned along with the sample waveguide it is ready to pattern the cladding material over the waveguide. The waveguide is moved slowly along the length of the waveguide with the computer observed under the electron microscope and placed below the pipette which is just few microns above the waveguide. The whole waveguide is slowly patterned with the cladding material being dropped by reducing the pressure of the pressure controller and the patterned waveguide is cured and tested with the characterization setup for testing its working. The sample is first tested to check the thickness of the cladding material and observing the pipette and working of the whole process is finalized with adjustments by doing many runs of the whole setup. Finally, the actual SU-8 waveguide is run through the experiment and NOA61 as a cladding is patterned.

3.7 Theory of Thickness and Index of Refraction Measurement

Prism coupler Model 2010/M from Metricon corp. [42] is used to measure thickness and index of refraction of a waveguide over conventional methods based on ellipsometry and spectrophotometry. It uses advanced optical waveguiding techniques to rapidly and accurately measure both thickness and refractive index/birefringence of dielectric and polymer films. The prism coupler module is explained in detail,

3.7.1 Prism coupler model 2010 module

The model 2010 prism coupler is comprised of three major component modules as shown in the Figure 16,

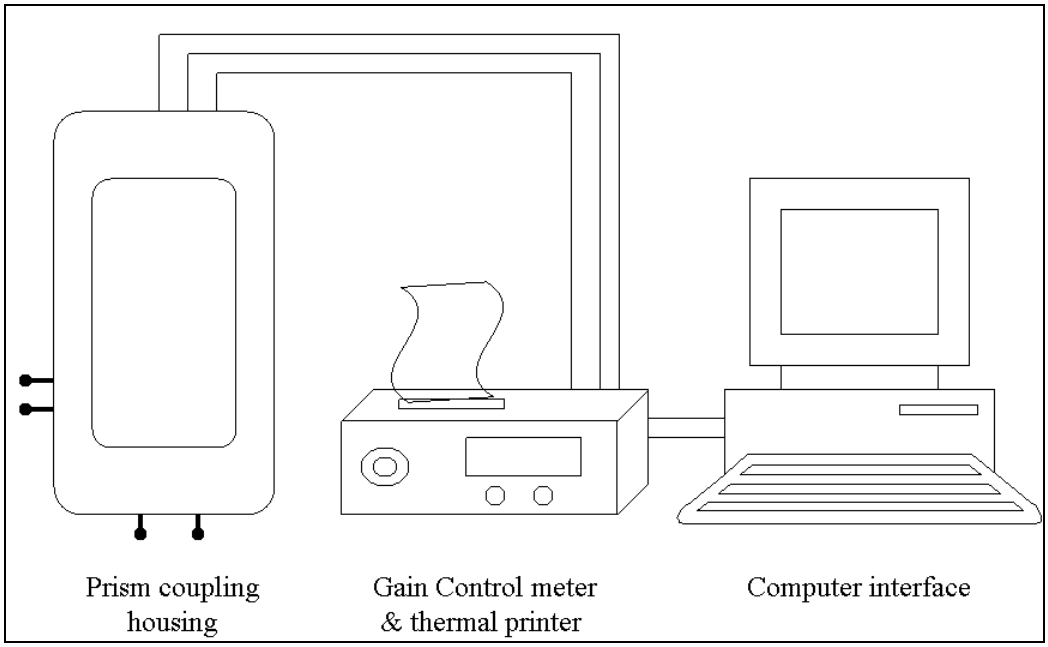

Figure 16: Prism coupler Model 2010/M module.

a) An optics module which houses the laser, rotary table, prism and other components necessary to excite the film propagation modes.

b) A PC (including video terminal, printer and mouse) which acquires displays and analyzes mode patterns and calculates results.

c) An interface module which connects the optics module and the PC and which incorporates the system's analog amplifiers and step motor drive electronics.

The principal components of the optics module consist of one or more lasers, a reference slit, a position adjustment mirror and a rotary table upon

which the coupling prism and primary photodetector are mounted. The laser beam first passes through a small defining aperture and is then directed onto the coupling prism by the adjustable mirror. The rotary table is driven by a stepper motor and the angular position of the table is displayed on the PC's video display. When power is first applied, the table must be "referenced", i.e., the counter which displays the table position must be made to reflect the actual angular position of the table. This is accomplished by placing a reference slit and photodetector adjacent to the beam defining aperture and using slit/detector combination to sense the laser beam strikes the entrance face of the prism perpendicularly. When this condition occurs, some light is retroreflected back along the laser path, passes through the reference slit, and illuminates the reference photodetector. When intensity of light striking the reference photodetector reaches maximum intensity, the counter which displays the angular position of the table is set to zero. The Figure below shows the prism housing inside the prism coupler and the procedure to use prism coupling is explained.

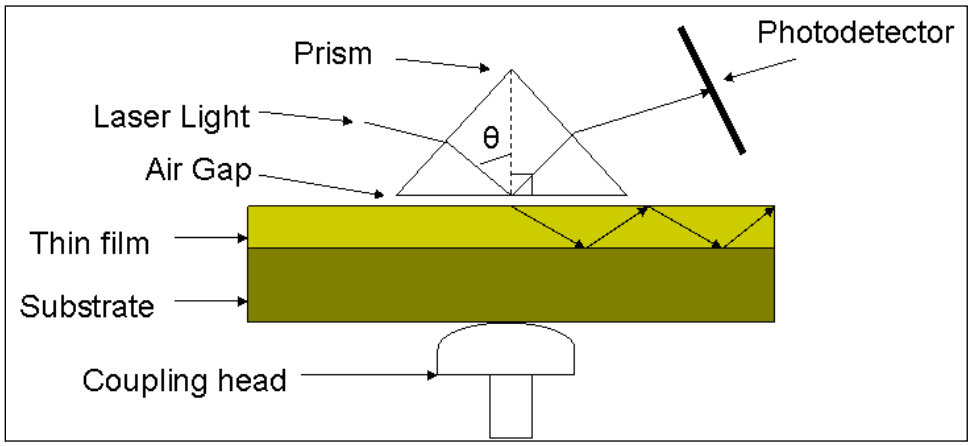

Figure 17: Theory of prism coupling.

A laser beam strikes the base of a high refractive index prism and is reflected onto a photodetector. The film to be measured is brought into contact with the prism base by means of a pneumatically-operated coupling head so that the air gap (typically less than 100-200 nm and caused by the roughness of the two surfaces) separates the sample and the prism. The angle of incidence, θ, of the laser beam can be varied by means of a rotary table upon which the prism, film, coupling head and photodetector are mounted. At certain values of θ, called mode angles, photons violate the total internal reflection criterion, and tunnel from the base of the prism across the air gap and into the film and enter into optical propagation modes, causing a sharp drop in the intensity of light striking the photodetector.

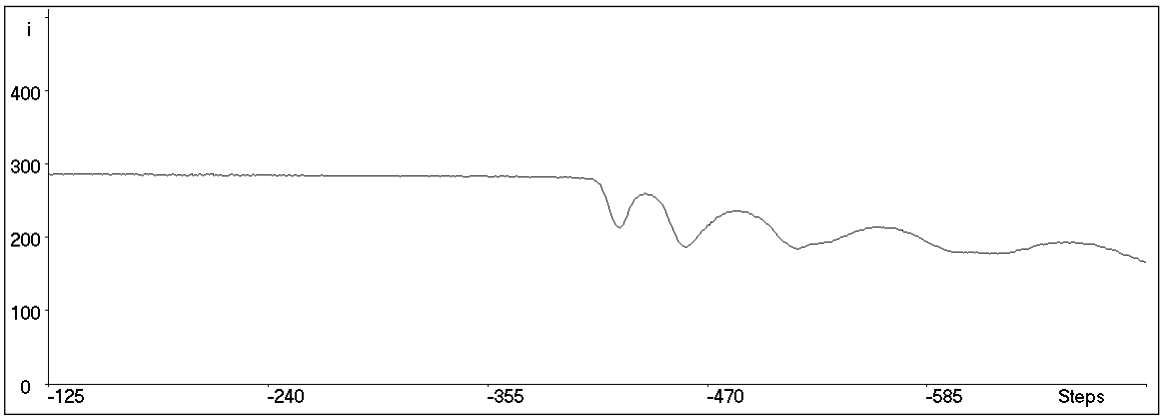

Figure 18: Example of thickness measurement.

If the intensity striking the photodetector is plotted as a function of the angle θ, a characteristic similar to the one above will be obtained. For a given substrate type, angular location of the modes depends only on the film thickness and index. Thus as soon as two mode angles are measured, the film thickness and index can be calculated by an appropriate computer algorithm. For the mth mode (where m=0 for the leftmost mode), the following eigenvalue equation, commonly referred to as the “mode equation” holds:

$$(2\pi/\lambda)*n\cos(\theta_2)*T + \psi 10 + \psi 12 = m\pi$$

Where,

λ is the wavelength,

n is the film index,

T is the film thickness, and

ψ10 and ψ12 are the Fresnel phase shifts at the film-air and film-substrate interfaces.

The above equations are complex transcendental equations which must be solved numerically, but simultaneous solution of the equations for two modes yields the thickness and the index of the film.

If more than two modes are observed, the problem is overspecified and it is possible to calculate independent thickness estimates from each pair of modes and the mean and standard deviation of all the estimates. Thus, a standard deviation will be calculated for both thickness and index for films which are thick enough to support three or more modes. As long as thickness standard deviation is low (less than 1-2 %) there is a little doubt the reliability of the measurement since it is virtually impossible for any significant operator or hardware error to occur without causing the thickness standard deviation to rise above 1-2% range.

The standard deviation results are useful checks on the self-consistency of the technique. They also provide a semi-quantitative indication of refractive index nonuniformity with depth, since mode positions of films with an index gradient vary slightly from mode positions of a film with uniform index vs. depth. When the perturbed mode positions of a film with an index gradient are fed into the analysis software (which assumes a zero-gradient film) the individual thickness and index estimates generated for each pair of modes disagree slightly and the standard deviation results rise above a background level.

With rare exceptions, mode spectra for single films manifest certain common characteristics, a) The first mode (most positive angle) is relatively shallow but sharp, and successive modes become deeper and broader, b) The

mode spacing become greater as θ, the coupling angle, becomes more negative, c) For a given thickness, as the index increases, the mode pattern shifts to the left (more positive theta), and d) for a given film thickness, as the index increases, the mode pattern shifts to the left (more positive theta), and for a given index as thickness decreases, the modes become more widely spread apart. (This last phenomenon gives rise to the minimum thickness limitation of the technique, since fewer and fewer of the modes are observable as mode spacing increases.) If additional force is applied to the coupling head to clamp the sample to the prism more tightly, coupling efficiency increases and the mode spectrum deepens.

While the depth of the modes may be changed by a number of factors (increased coupling pressure, improved optical alignment), the mode angle positions for a given film are normally quite stable. An exception to this is relatively thin films of relatively low index materials on higher index substrates (e.g. films on SiO_2 thinner than 1-2 microns on silicon) for which the mode positions do exhibit some shifting if the size of the air gap becomes too small. If uncontrolled, such shifts can degrade the accuracy of the thickness measurement, although index accuracy is only slightly affected. The prism coupler defines the effective index [42] which is the theory used for calculating and measuring the index of fraction and thickness of thin films.

3.7.2 Definition of effective index (β – value)

β – value, for optical propagation modes, each mode is characterized by a very well defined angle of incidence on the base of the prism, the β value for light impinging at any angle θ_1 on the base of a prism with index n_p is simply defined as

$$\beta(\theta) = n_p \sin(\theta_1)$$

More generally, the β value for any ray of light is simply nsin(θ) where n is the index of the medium in which light is travelling and θ is the angle of incidence it makes on the boundary of the material as it is refracted into the next material. Since, by snell's law,

$$n_1 \sin(\theta_1) = n_2 \sin(\theta_2)$$

β values are preserved when a ray of light is refracted at the boundary between two media. Moreover, when photons tunnel from the base of the prism into the film optical propagation mode, they behave they are refracted at the prism/film interface, so snell's law is obeyed, and the β value of the light ray is unchanged between the prism and the film.

In addition, if the coupling (acute) angle of the prism is known, it is easy to calculate the angle of incidence of the light on the base of the prism for any angle of incidence on the entrance face. Thus the β value for any mode can be calculated from the angle which the light makes with respect to the prism entrance face when the mode is observed.

The β value is important because it allows calculation of the Fresnel phase shifts (ψ10 and ψ12). If two β values can be measured experimentally, ψ10 and ψ12 can be determined and an eigenvalue equation can be used to determine the thickness and index of the thin film. Thus the prism coupling technique provides a method for measuring β values for the film modes and then substituting these values into the mode equation to permit calculation of thickness and refractive index.

The β value is also useful in determining when total internal reflection occurs. When light impinges on the prism base, for example, by snell's law it cannot be refracted into the adjacent film (or enter into an optical propagation mode) until the β value drops below the film index, Thus, the β values for all film modes must be lower than the film index. In addition, for the case of a dual film with higher index film on top, it is possible to predict that for modes with β values above the lower film index the light will be totally reflected at the upper/lower interface. Similarly, for a single film on a substrate of lower index, modes with β values higher than the substrate index will be totally reflected at the film-substrate interface.

In summary, the β values are the raw materials which permit the calculation of film parameters by the prism coupling technique. For any mode, the β value is simply np sin(θ1) where np is the index of the prism and θ1 is the angle of incidence which the light makes on the base of the prism when the mode is observed. Finally, the β value for any mode may not exceed the film

index, and if the β value is higher than the index of substrate or film directly below, the light will be confined in the film as a result of total internal reflection at the lower boundary of the film. The Metricon model 2010/M prism coupler is summarized below explaining its housing and working. In the further sections, the results of the experiments performed using the above methodology is discussed in detail.

CHAPTER 4
RESULTS

4.1 Power Loss Calculations for SU-8 Waveguide

The SU-8 polymer is ensured for low optical propagating loss before fabricating the actual waveguide. The SU-8 waveguide is tested using the prism coupler to ensure the guiding of light through the length of the core. The prism coupler houses a visible red laser source of 633nm wavelength and is subjected to this light source and power adjustments are performed to observe a bright light streak across the SU-8 waveguide sample, shown in Figure 19. The light passes across the length of the waveguide ensuring the passage of energy through the SU-8 polymer. The bright red streak across the length of the waveguide shows that polymer SU-8 guides the light effectively confirming the working of MZI with SU-8 as the core layer.

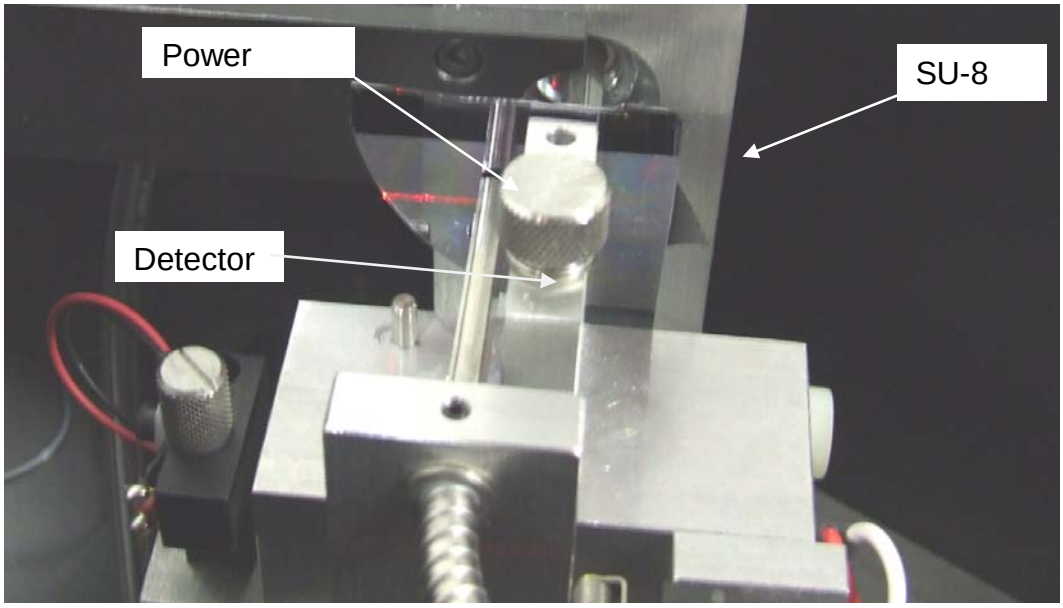

Figure 19: Power across the SU-8 thin film.

Further, power loss calculations are done which enables us to test the working of the waveguide using prism coupler following the steps provided in the manual. The prism coupler measures loss in the SU-8 optical waveguide using the moving fiber method in which the exponential decay of light is measured by a fiber probe scanning down the length of the propagating streak. An essential requirement for loss measurement is that the film to be evaluated be a guiding structure that is the lower cladding on which the core is deposited should have a refractive index lower than core. A least squares fit is then made to the intensity vs. distance pattern and the loss is calculated in db/cm. This method works well for the SU-8 optical waveguide developed by LDW because. a) The guide has some scattering loss to provide a means of sampling the light intensity which remains within the waveguide at each point and b) the scattering properties are spatially uniform (i.e., the scattering efficiency is same along the length of the

propagating streak). The overall loss measured is the combined total of both scattering loss (from particles or other scattering centers and surface roughness) and loss due to the inherent absorption of the waveguide material. Figure20 shows the power loss of 0.77dB/cm through the SU-8 waveguide on a silicon substrate with silicon oxide as the lower cladding.

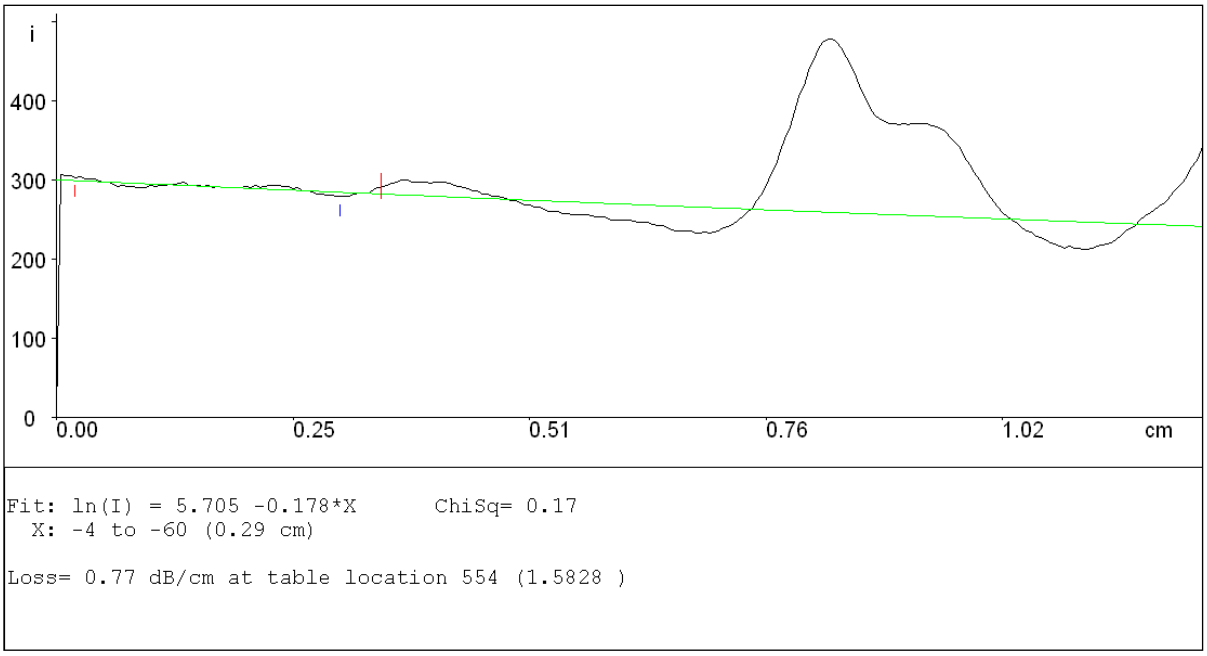

Figure 20: Power loss calculation from the prism coupler.

The power loss calculation results prove that a working waveguide can be fabricated using LDW in the laboratory with polymer SU-8 with less 1db/cm loss. The fabricated SU-8 waveguide is further coated with an upper cladding of polymer NOA 61. NOA61 has a refractive index of 1.56 measured using the prism coupler. This upper cladding is coated using fountain pen micropatterning methodology. The results of this methodology are compared with another

waveguide developed by coating the upper cladding using the spin coating technology. The testing of these waveguides to obtain the output patterns are done through a characterization setup whose results prove the working of the MZI developed using the LDW and fountain pen micro-patterning.

4.2 Physical Characteristics of the Micro-patterned SU-8 Waveguide

4.2.1 Refractive index

A SU-8 thin film is developed using the Spin coating process on a silicon substrate having a lower cladding of Silicon oxide that is the core layer of the guiding waveguide. The lower cladding has a refractive index of 1.46 and thickness of 2 microns verified by the prism coupler measurements. This core layer of the waveguide is further designed and fabricated using the LDW system to get a straight waveguide with dimensions less than 10 microns. The refractive index is measured using the prism coupler following the guidelines provided for performing the calculations (section 3.7). The refractive index of the SU-8 thin film on silicon oxide substrate is found to be 1.5957 and is very stable with 0.002% of standard deviation (SD) as shown in the Table 1.

Table 1: Uniformity of refractive index of SU-8 samples.

Sample	Refractive index
1	1.5958
2	1.5958
3	1.5955
4	1.5958
5	1.5959
Mean	1.59576
SD	0.0002

4.2.2 Thickness of the SU-8 Waveguide

The SU-8 core layer is developed using spin coating and the thickness of the SU 8 thin film is calculated to be 5 microns with less than 1% of standard deviation, that is the height of the SU-8 waveguide is 5 microns. The thickness measurements [Appendix D] are done using the prism coupler with different samples; the thickness mean is calculated as shown in the Table 2. A SD of 0.1582 verifies the uniformity of developing the core layer with a thickness of 5 microns. Thus, the height of the SU-8 waveguide is confirmed to be 5 microns.

Table 2: Thickness uniformity of SU-8 thin film.

Sample	Thickness (microns)
1	5.2861
2	4.9782
3	4.8674
4	5.0481
5	4.9589
Mean	5.02774
SD	0.1582

4.2.3 Width of the SU-8 Waveguide

The SU-8 thin film is to be fabricated using LDW to get a width of 5 microns to develop a waveguide less than 10 microns. The experiment is started using the minimum filter 1A and with minimum speed of 1mm/sec of the precision stage and is controlled in the G code program (Appendix A). The width of the waveguide is very large around 50 microns when observed under the electron microscope. The image of the waveguide designed using the LDW system and observed under the electron microscope with 20X magnification

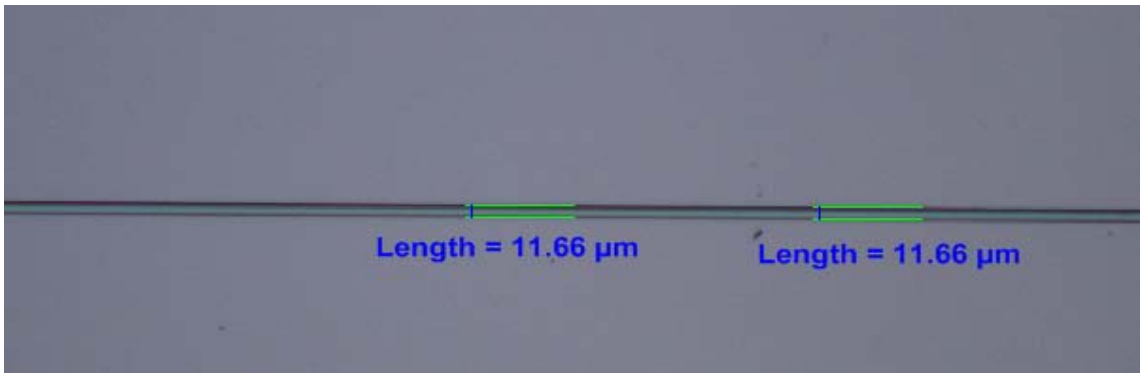

Figure 21: SU-8 waveguide with a width of 12 microns.

The objective in the LDW set-up is adjusted several times during the experimentation to ensure the maximum laser power focusing on the translational stage plane. The filter power is increased slowly upto 5A and the speed is increased upto 5mm/sec in a matrix pattern to get the width dimension less than 10 microns. The waveguide dimensions vary and decrease upto 20 microns using the 5A filter and at a speed of 5mm/sec. 5A filter is fixed and same is true for the speed above 5mm/sec. the width of the waveguide is still above 10 microns. The width of the SU-8 waveguide is around 12 microns with 5A filter and a speed of 5.5mm/sec, as shown in the Figure 21.

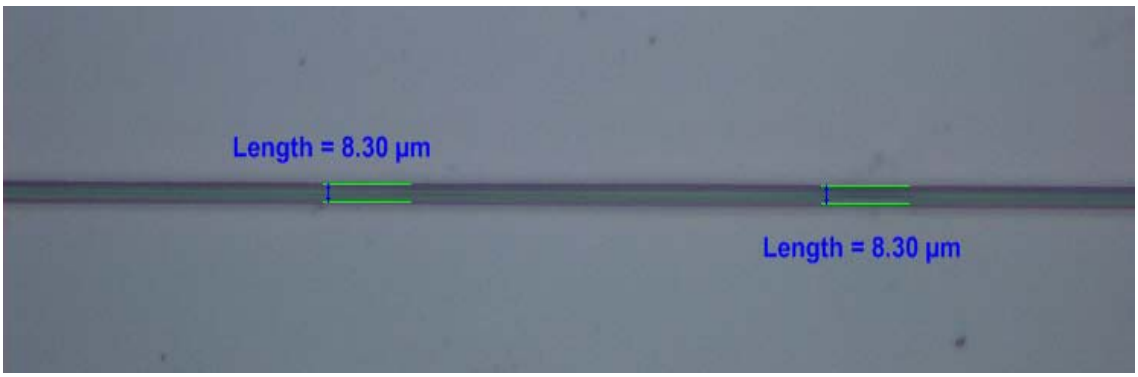

Figure 22: SU-8 waveguide with 8 microns width.

The focusing of the waveguide is adjusted minutely at this stage to get a better waveguide and is done in clockwise and anticlockwise directions to get the best focusing, at higher speeds the quality of the waveguide developed decreases resulting in not so good quality of waveguides.

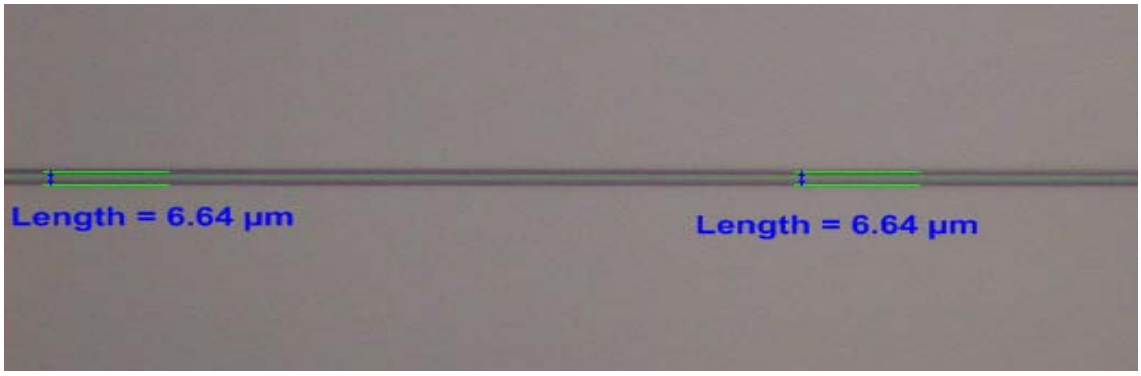

Figure 23: SU-8 waveguide with width of 6 microns.

To improve the width of the waveguide, the filter is increased to 6A since with a better focusing laser point on the waveguide placed on the translational stage. Also, doing this gets the width below 10 microns. Waveguide with 8 microns of width is fabricated at 6A filter and 5.5mm/sec, shown in Figure 22.

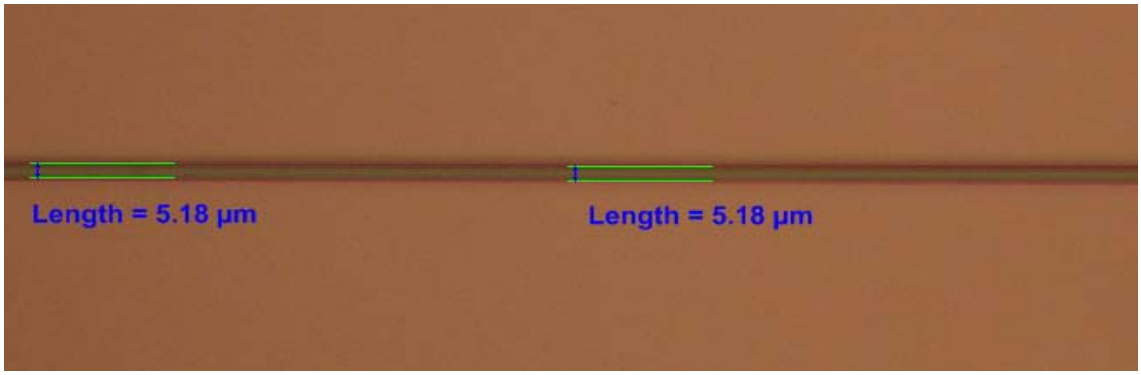

Figure 24: SU-8 waveguide with width of 5 microns.

Increasing the speed slowly further gives a waveguide with 6 microns dimension of very good quality shown in Figure23. Finally at the speed of 7mm/sec using the filter 6A, SU-8 waveguide with 5 microns is fabricated. Figure 24 and 25 show the waveguide dimension seen under the electron microscope. The sample fabricated at 7mm/sec speed with 6A filter is an excellent straight

waveguide with brittle walls and the result is stable and duplicated. This experiment is run multiple times with a silicon oxide layer as the substrate to confirm the result.

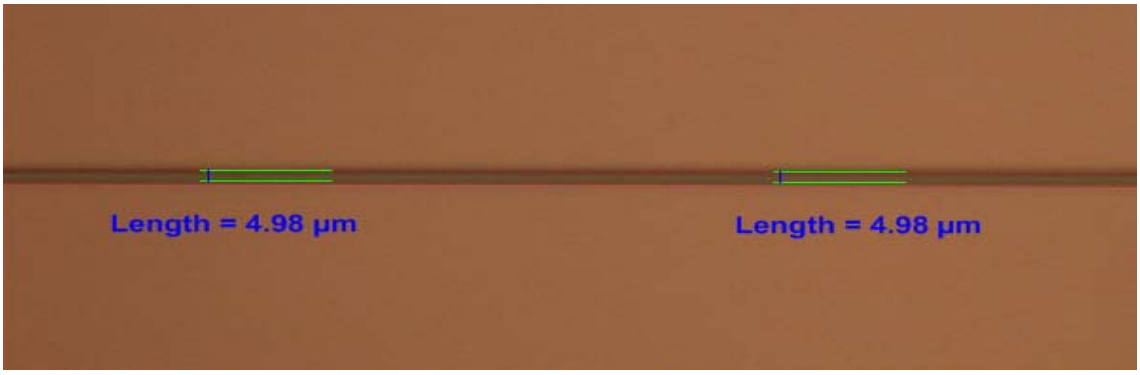

Figure 25: SU-8 waveguide 5 microns wide.

The fabrication of the SU-8 waveguide is very rigorous due to the requirement of developing the device with dimensions in few microns. The LDW set-up is less stable with the focusing point getting displaced very frequently, causing frequent adjustments in the set-up for proper results. Even a minute change in the focusing of the laser source causes a difference of few microns in the width of the waveguide. Also, the surrounding environment causes variations in the quality of the device being fabricated. The polymer being sensitive to light affects the functionality of the waveguide with minor variations in conditions in the laboratory.

To verify the results of LDW for fabricating a 5X5 SU-8 straight waveguide is scanned through a scanning electron microscope (SEM), an SEM image is shown in Figure 26 verifying the dimensions of the fabricated waveguide. SEM is a type of electron microscope that images the sample surface by scanning it with

a high-energy beam of electrons in a raster scan pattern. The electrons interact with the atoms that make up the sample producing signals that contain information about the sample's surface topography, composition and other properties.

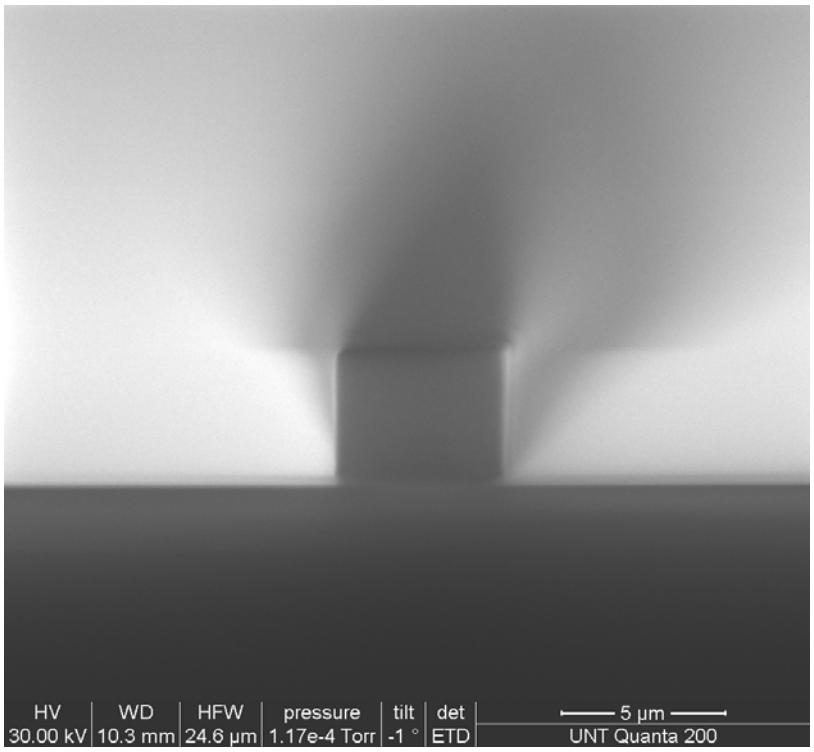

Figure 26: SEM image of the developed waveguide.

The SU-8 straight waveguide developed in Figure 26 is further processed to pattern an upper cladding using fountain pen micro-patterning and spin coating whose results are compared using the characterization setup designed for the fabricated waveguides.

4.3 Characterization of Micro-Patterned SU-8 Waveguide

The SU-8 waveguide is designed and fabricated using the LDW system, the upper cladding is patterned using two methods, a) fountain pen micropatterning and b) spin coating method. The output results are compared using both methods to verify the functioning of fountain pen micropatterning and its ability for developing chemically/biological sensor arrays. A characterization setup is designed and put together for testing the effective working of the sample, the characterization setup used is shown in Figure 28,

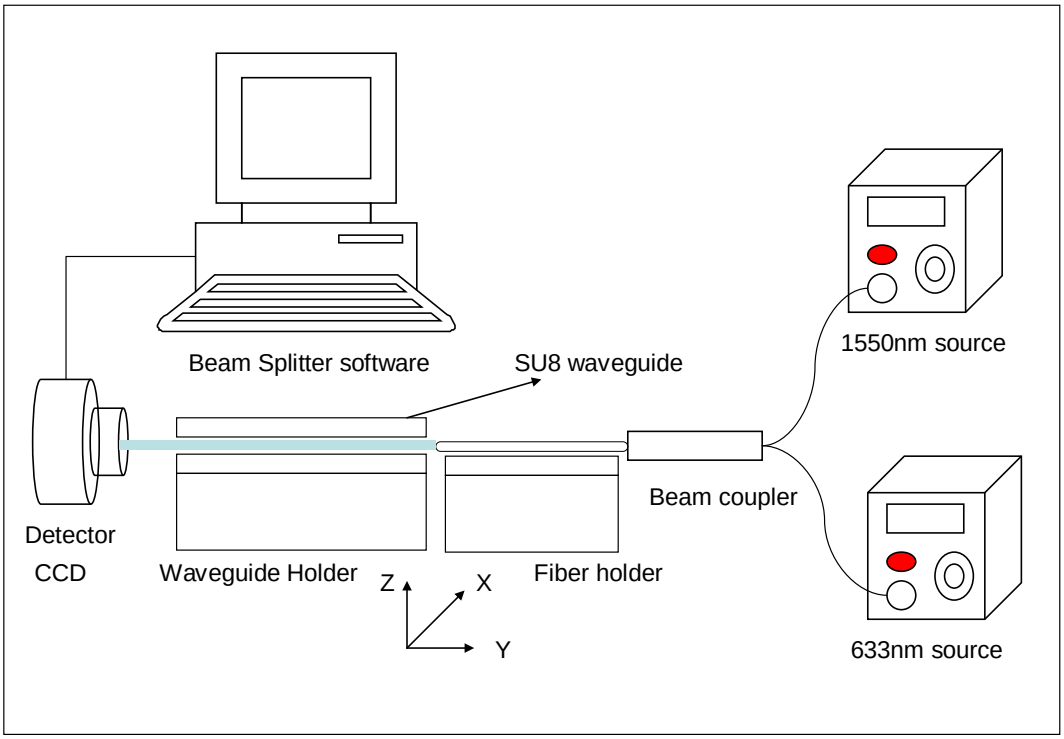

Figure 27: Characterization set-up.

The characterization set up consists of two laser sources of 633nm and 1550nm wavelength connected to the optical fiber via 2:1 beam coupler. The fiber is placed on a 4 axis fiber holder to control its movement in X, Z. It is placed

ahead of another 3 axis holder which holds the waveguide sample and controls its movement in X, Y, Z directions. In total we have 5 axes controls to precisely adjust the sample in the line of the fiber to couple the light in the waveguide. The light is coupled in using the visible laser at 633nm doing fine adjustments to get perfect alignment of the laser through the length of the waveguide. The visible light source is switched with the 1550nm laser source and fine tuning in alignment is done to get the output across the length of the waveguide.

The working of the waveguide is analyzed using the characterization setup shown in Figure 27, the light is coupled in the waveguide with a laser source of 1550 nm at the input and collecting the light at the other end of the waveguide using a CCD camera which runs through a Laser beam analyzer software [42]. The laser beam analyzer gives the results and displays the output modes of the fabricated waveguide. The working of the waveguide is explained based on the close resemblance of the displayed modes at 1550nm wavelength with that of the fundamental mode obtained by the BeamPROP simulation software. In general terms, the waveguide is said to be working and functioning correctly if clear and distinct modes are observed at the output of the waveguide. The output resultant modes of the waveguide are shown in two and three dimensional views.

The output waveguide patterns show that the light at 1550 nm wavelength has been coupled through the waveguide and it guides the light through its length to reach the output. The results of the waveguide developed using fountain pen micropatterning for patterning the upper cladding prove that fountain pen

micropatterning can be used effectively for developing waveguides and devices for printing multiple materials on the same base to develop sensor arrays and related applications. Also, additionally to prove the results of the waveguide developed by the simple micro-fabrication technique of LDW and fountain pen micro-patterning are compared with the results of the waveguide developed using micro-fabrication technique of LDW and spin coating.

Output modes for a waveguide developed using LDW with upper cladding fabricated using fountain pen micropatterning technology [Appendix C],

The output modes as seen in a 2 dimensional view,

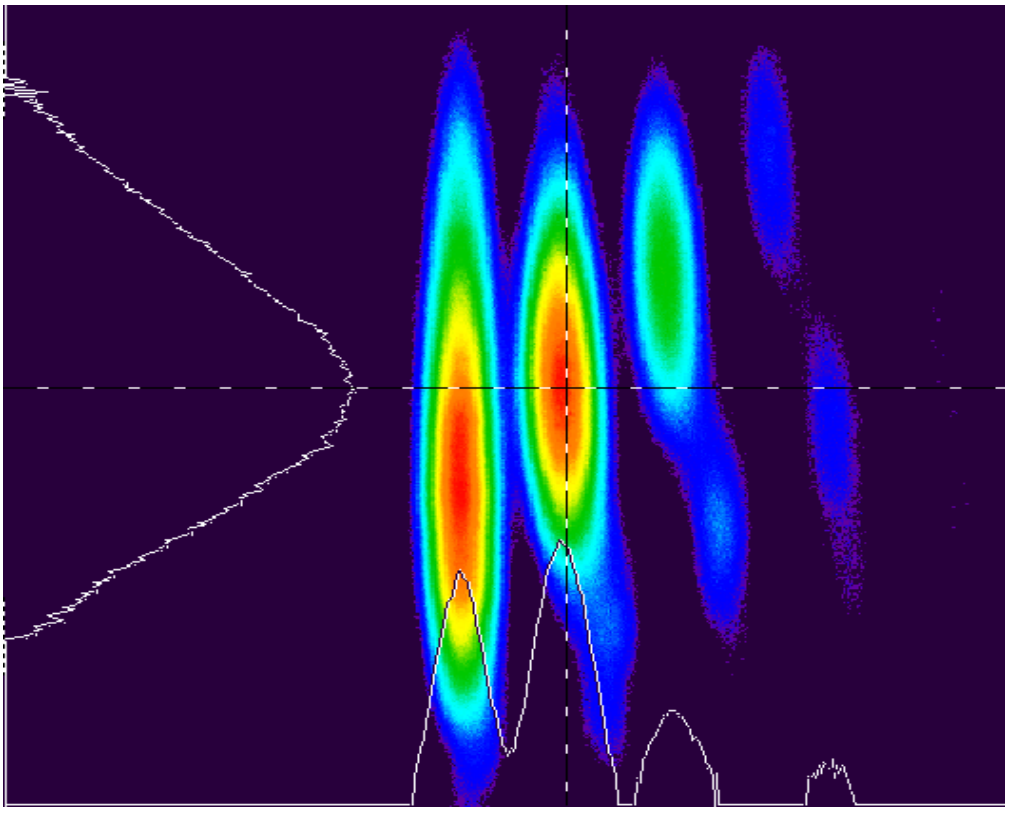

Figure 28: 2D image of output modes of waveguide with upper cladding patterned using fountain pen micropatterning.

The output modes as seen in a 3 dimensional view,

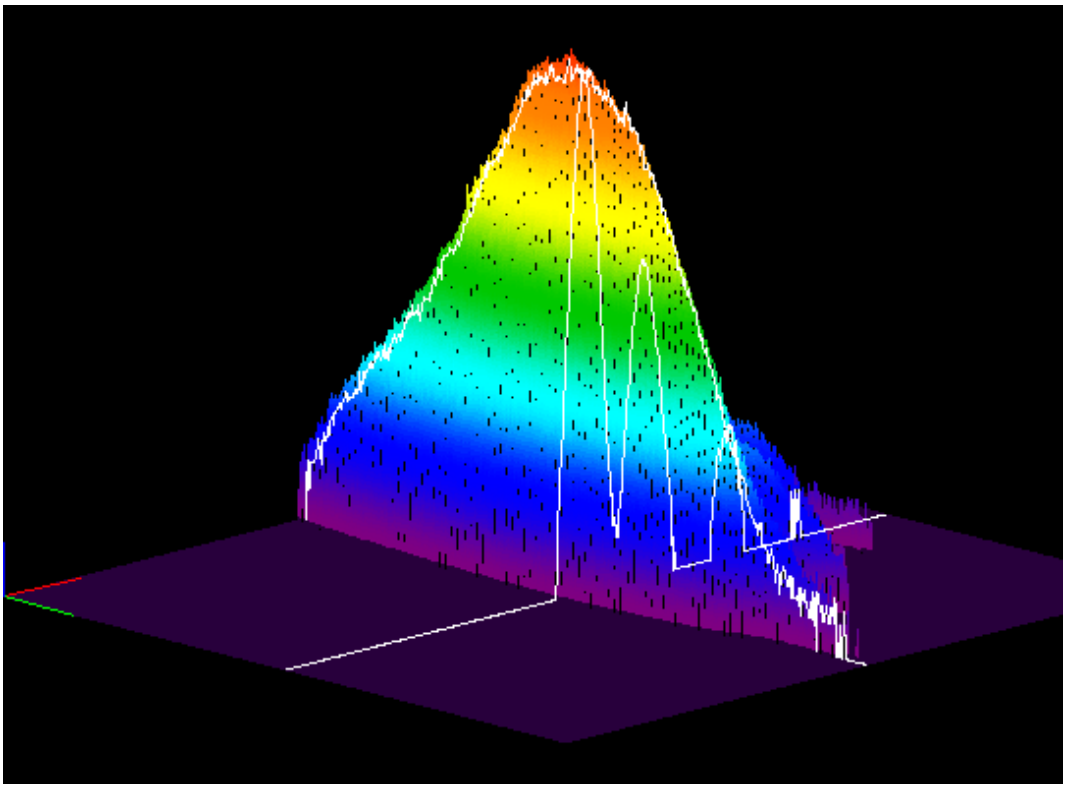

Figure 29: 3D image of output modes of waveguide with upper cladding patterned using fountain pen micropatterning.

Output modes for a waveguide developed using LDW with upper cladding fabricated using spin coating technology [Appendix B].

a) The output modes as seen in a 2 dimensional view,

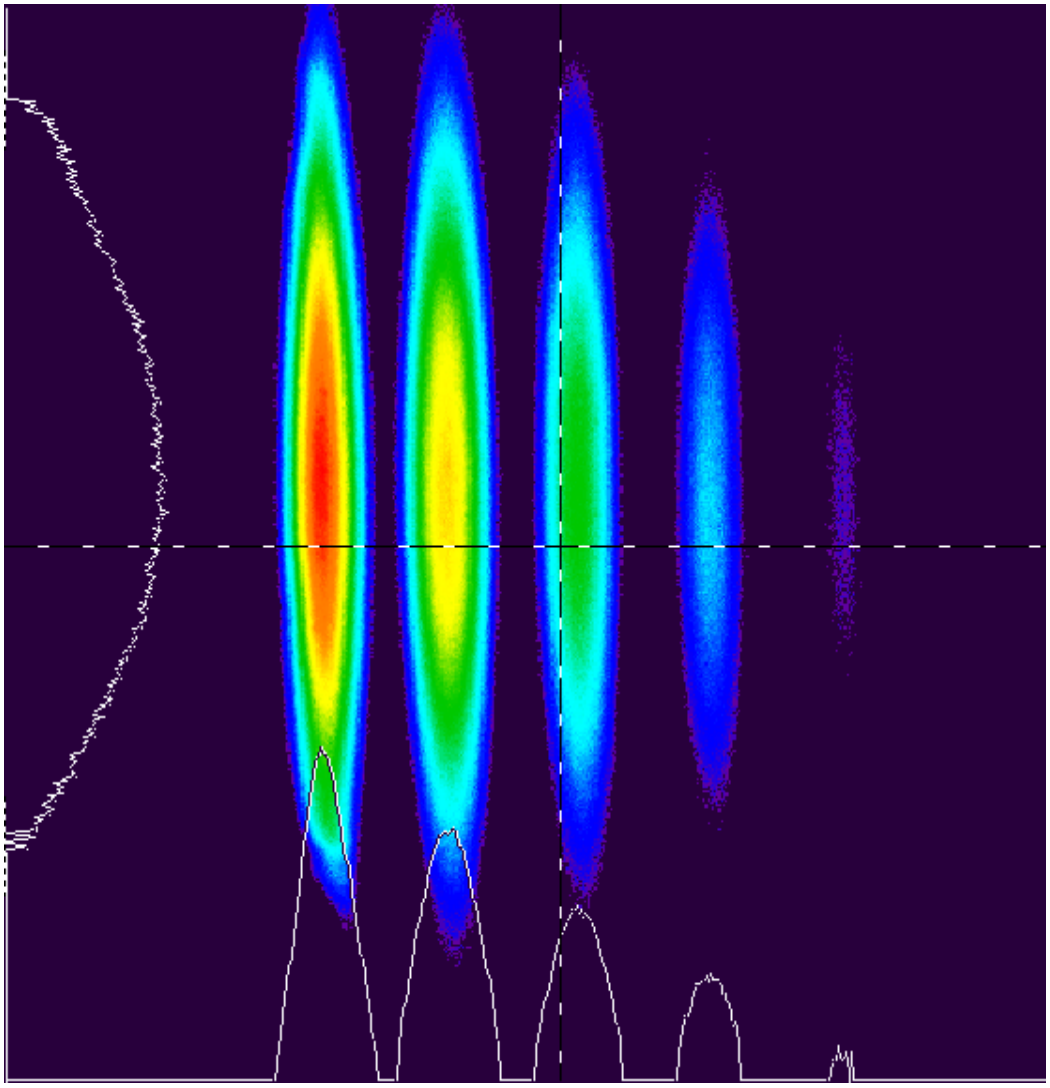

Figure 30: 2D image of output modes of waveguide with upper cladding patterned using spin coating.

The output modes as seen in a 3 dimensional view,

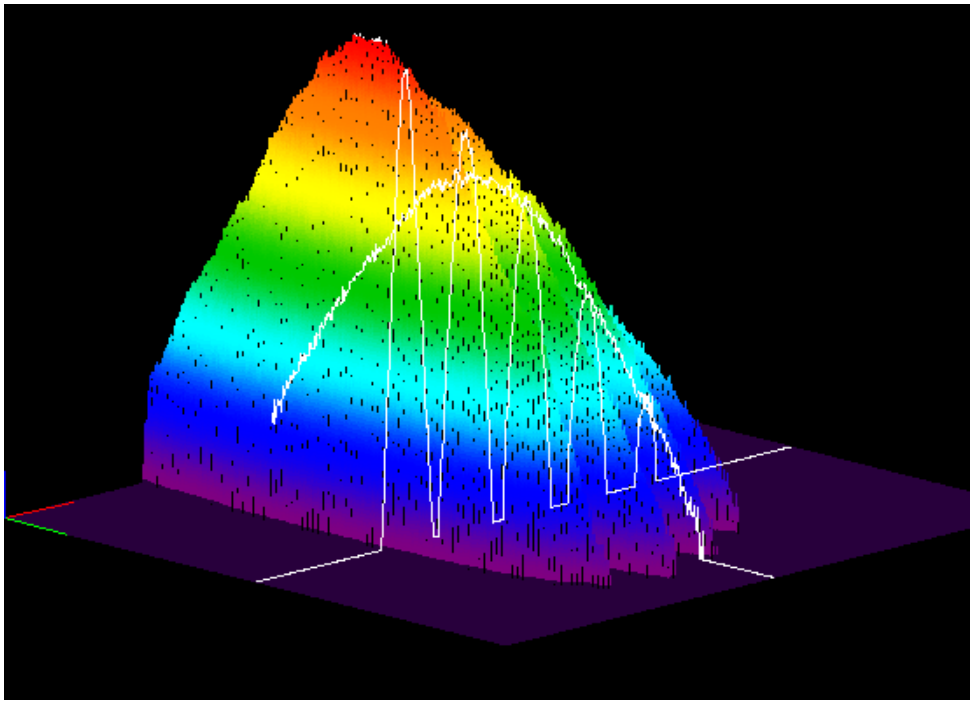

Figure 31: 3D image of output modes of waveguide with upper cladding patterned using spin coating.

The output patterns of both the waveguides with upper cladding developed using fountain pen micropatterning and spin coating are compared and the output modes obtained verify the their functionality and proves that fountain pen micropatterning can be used to pattern the upper cladding of a waveguide and used to develop the MZI interferometers for chemical/biological sensor arrays.

CHAPTER 5

CONCLUSION

5.1 Summary

A maskless micro-fabrication technique is developed combining of LDW and fountain pen micropatterning for developing polymer based sensor arrays that are compact, highly sensitive and user friendly. This technique can be effectively used to develop single sensor prototypes and designs.

Microfabrication of a waveguide was achieved using the combination of LDW and fountain pen micropatterning using the polymer SU-8 as the core material with NOA61 as the upper cladding and silicon oxide as the lower cladding. The results prove that micro-fabrication technique of LDW and fountain pen micropatterning can be used to develop the MZI for chemical/biological sensing applications with a minimum waveguide propagation loss. A simplified micro-fabrication technique is developed for developing and designing prototype chemical/biological sensor arrays. Comparable performance was achieved with the much simplified fabrication process. This technique can thus replace the multi step photolithography process by the LDW and fountain pen micropatterning for fabricating IO devices.

Some of the highlights of this research are given as follows,

- LDW technology is set-up successfully in the laboratory for fabricating waveguides on silicon and glass substrates.

- SU-8 waveguide with less than 10 microns in width and height was fabricated using maskless technique of LDW.
- Results of LDW are verified through SEM.
- The fabricated SU-8 waveguide has a propagation loss of less than 1db/cm.
- Fountain pen micro-patterning set-up is tested for patterning cladding layers on straight waveguides.
- The fabricated SU-8 waveguide is patterned with NOA 61 upper cladding using fountain pen micro-patterning and spin coating methodology.
- A characterization setup is developed with dual laser sources for testing the developed waveguides.
- Satisfactory characterization results are obtained from the SU-8 waveguides developed using fountain pen micro-patterning and spin coating.
- A highly simplified micro-fabrication technique for developing IO devices has been implemented.
- Fountain pen micropatterning is successfully implemented with LDW for developing sensor arrays for chemical/biological sensing.

APPENDIX A

G-CODE PROGRAMS

G code programs

1.) G code program, writes 6-6cm lines at 6.5mm/s dwell speed with 50um distance between two lines

```
DVAR $fil
$fil = FILEOPEN "COM1", 2
COMMINIT $fil, "baud=9600 parity=N data=8 stop=1"
COMMSETTIMEOUT $fil, -1, 0, 0  ; Define 1 second timeout for data at serial
port
ENABLE X Y          ; turn on servo loop control for the axes
METRIC              ; set to use metric programming units
SECONDS             ; speeds interpreted as units / second
ABSOLUTE            ; set absolute programming mode
INCREMENTAL         ; set Incremental programming mode
RapidFeedRate.X = 6.5
RapidFeedRate.Y = 6.5
LINEAR X50 Y90 F30        ;        starting position x=50, y=90
DWELL 0.5
FILEWRITENOTERM $fil, "ens\x0D"              ;shutter open
RAPID X30 F1
FILEWRITENOTERM $fil, "ens\x0D"              ;shutter closed
DWELL 1
RAPID Y-1 F1
DWELL 0.1
FILEWRITENOTERM $fil, "ens\x0D"              ;open
RAPID X-30 F1
FILEWRITENOTERM $fil, "ens\x0D"              ;closed
DWELL 1
RAPID Y-1 F1
DWELL 0.1
FILEWRITENOTERM $fil, "ens\x0D"              ;open
RAPID X30 F1
FILEWRITENOTERM $fil, "ens\x0D"              ;closed
DWELL 1
RAPID Y-1 F1
DWELL 0.1
FILEWRITENOTERM $fil, "ens\x0D"              ;open
RAPID X-30 F1
FILEWRITENOTERM $fil, "ens\x0D"               ;closed
DWELL 1
RAPID Y-1 F1
DWELL 0.1
FILEWRITENOTERM $fil, "ens\x0D"              ;open
```

```
RAPID X30 F1
FILEWRITENOTERM $fil, "ens\x0D"              ;closed
DWELL 1
RAPID Y-1 F1
DWELL 0.1
FILEWRITENOTERM $fil, "ens\x0D"              ;open
RAPID X-30 F1
FILEWRITENOTERM $fil, "ens\x0D"              ;closed
FILECLOSE $fil
DWELL 0.1
HOME X Y
```

2.) G code program, writes 24-6cm lines at 6.5mm/s dwell speed with 50um distance between two lines

```
DVAR $fil
$fil = FILEOPEN "COM1", 2
COMMINIT $fil, "baud=9600 parity=N data=8 stop=1"
COMMSETTIMEOUT $fil, -1, 0, 0 ; Define 1 second timeout for data at serial port
ENABLE X Y          ; turn on servo loop control for the axes
METRIC              ; set to use metric programming units
SECONDS             ; speeds interpreted as units / second
ABSOLUTE            ; set absolute programming mode
INCREMENTAL         ; set Incremental programming mode
RapidFeedRate.X = 6.5
RapidFeedRate.Y = 6.5
LINEAR X50 Y90 F30                ;starting position x=50, y=90
DWELL 0.5
FILEWRITENOTERM $fil, "ens\x0D"  ;shutter open
RAPID X50 F1
FILEWRITENOTERM $fil, "ens\x0D"  ;shutter closed
DWELL 1
RAPID Y-1 F1
DWELL 0.1
FILEWRITENOTERM $fil, "ens\x0D"       ;open
RAPID X-50 F1
FILEWRITENOTERM $fil, "ens\x0D"  ;closed
DWELL 1
RAPID Y-1 F1
DWELL 0.1
FILEWRITENOTERM $fil, "ens\x0D"  ;open
RAPID X50 F1
FILEWRITENOTERM $fil, "ens\x0D"  ;closed
DWELL 1
```

```
RAPID Y-1 F1
DWELL 0.1
FILEWRITENOTERM $fil, "ens\x0D"  ;open
RAPID X-50 F1
FILEWRITENOTERM $fil, "ens\x0D"  ;closed
DWELL 1
RAPID Y-1 F1
DWELL 0.1
FILEWRITENOTERM $fil, "ens\x0D"  ;open
RAPID X50 F1
FILEWRITENOTERM $fil, "ens\x0D"  ;closed
DWELL 1
RAPID Y-1 F1
DWELL 0.1
FILEWRITENOTERM $fil, "ens\x0D"  ;open
RAPID X-50 F1
FILEWRITENOTERM $fil, "ens\x0D"  ;closed
DWELL 1
RAPID Y-1 F1
DWELL 0.1
FILEWRITENOTERM $fil, "ens\x0D"  ;open
RAPID X50 F1
FILEWRITENOTERM $fil, "ens\x0D"  ;closed
DWELL 1
RAPID Y-1 F1
DWELL 0.1
FILEWRITENOTERM $fil, "ens\x0D"  ;open
RAPID X-50 F1
FILEWRITENOTERM $fil, "ens\x0D"  ;closed
DWELL 1
RAPID Y-1 F1
DWELL 0.1
FILEWRITENOTERM $fil, "ens\x0D"  ;open
RAPID X50 F1
FILEWRITENOTERM $fil, "ens\x0D"  ;closed
DWELL 1
RAPID Y-1 F1
DWELL 0.1
FILEWRITENOTERM $fil, "ens\x0D"  ;open
RAPID X-50 F1
FILEWRITENOTERM $fil, "ens\x0D"  ;closed
DWELL 1
RAPID Y-1 F1
DWELL 0.1
```

```
FILEWRITENOTERM $fil, "ens\x0D"  ;open
RAPID X50 F1
FILEWRITENOTERM $fil, "ens\x0D"  ;closed
DWELL 1
RAPID Y-1 F1
DWELL 0.1
FILEWRITENOTERM $fil, "ens\x0D"  ;open
RAPID X-50 F1
FILEWRITENOTERM $fil, "ens\x0D"  ;closed
DWELL 1
RAPID Y-1 F1
DWELL 0.1
FILEWRITENOTERM $fil, "ens\x0D"  ;open
RAPID X50 F1
FILEWRITENOTERM $fil, "ens\x0D"  ;closed
DWELL 1
RAPID Y-1 F1
DWELL 0.1
FILEWRITENOTERM $fil, "ens\x0D"       ;open
RAPID X-50 F1
FILEWRITENOTERM $fil, "ens\x0D"  ;closed
DWELL 1
RAPID Y-1 F1
DWELL 0.1
FILEWRITENOTERM $fil, "ens\x0D"  ;open
RAPID X50 F1
FILEWRITENOTERM $fil, "ens\x0D"  ;closed
DWELL 1
RAPID Y-1 F1
DWELL 0.1
FILEWRITENOTERM $fil, "ens\x0D"  ;open
RAPID X-50 F1
FILEWRITENOTERM $fil, "ens\x0D"  ;closed
DWELL 1
RAPID Y-1 F1
DWELL 0.1
FILEWRITENOTERM $fil, "ens\x0D"  ;open
RAPID X50 F1
FILEWRITENOTERM $fil, "ens\x0D"  ;closed
DWELL 1
RAPID Y-1 F1
DWELL 0.1
FILEWRITENOTERM $fil, "ens\x0D"  ;open
RAPID X-50 F1
```

```
FILEWRITENOTERM $fil, "ens\x0D"  ;closed
DWELL 1
RAPID Y-1 F1
DWELL 0.1
FILEWRITENOTERM $fil, "ens\x0D"  ;open
RAPID X50 F1
FILEWRITENOTERM $fil, "ens\x0D"  ;closed
DWELL 1
RAPID Y-1 F1
DWELL 0.1
FILEWRITENOTERM $fil, "ens\x0D"  ;open
RAPID X-50 F1
FILEWRITENOTERM $fil, "ens\x0D"  ;closed
DWELL 1
RAPID Y-1 F1
DWELL 0.1
FILEWRITENOTERM $fil, "ens\x0D"  ;open
RAPID X50 F1
FILEWRITENOTERM $fil, "ens\x0D"  ;closed
DWELL 1
RAPID Y-1 F1
DWELL 0.1
FILEWRITENOTERM $fil, "ens\x0D"  ;open
RAPID X-50 F1
FILEWRITENOTERM $fil, "ens\x0D"  ;closed
FILEWRITENOTERM $fil, "ens\x0D"  ;open
RAPID X50 F1
FILEWRITENOTERM $fil, "ens\x0D"  ;closed
DWELL 1
RAPID Y-1 F1
DWELL 0.1
FILEWRITENOTERM $fil, "ens\x0D"  ;open
RAPID X-50 F1
FILEWRITENOTERM $fil, "ens\x0D"  ;closed
DWELL 1
RAPID Y-1 F1
DWELL 0.1
FILECLOSE $fil
DWELL 0.1
HOME X Y
```

APPENDIX B

CHARACTERIZATION RESULTS WITH SPIN COATING

Characterization results showing the output power profile of MZI developed using LDW and spin coating.

Waveguide 1:

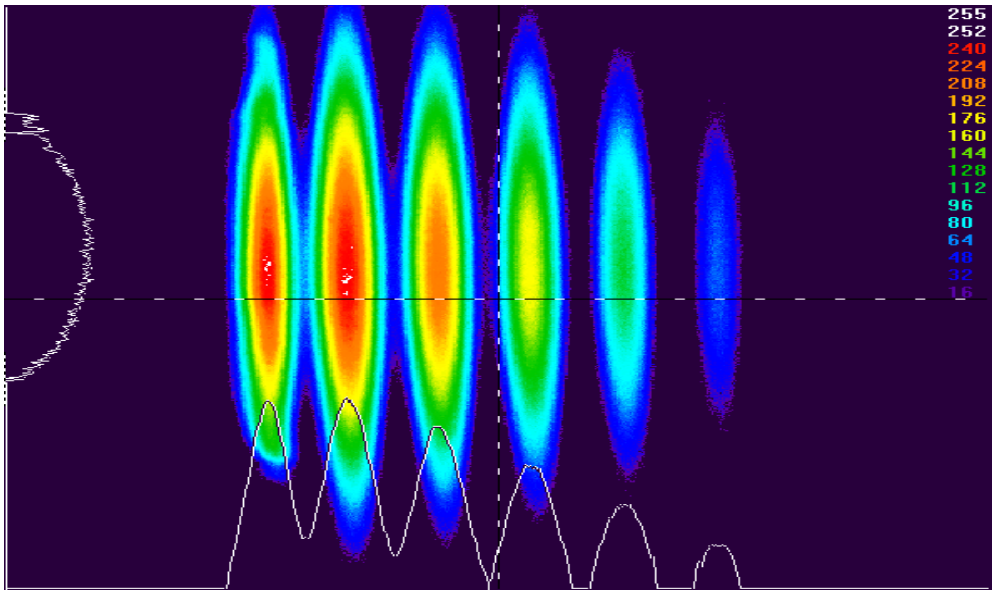

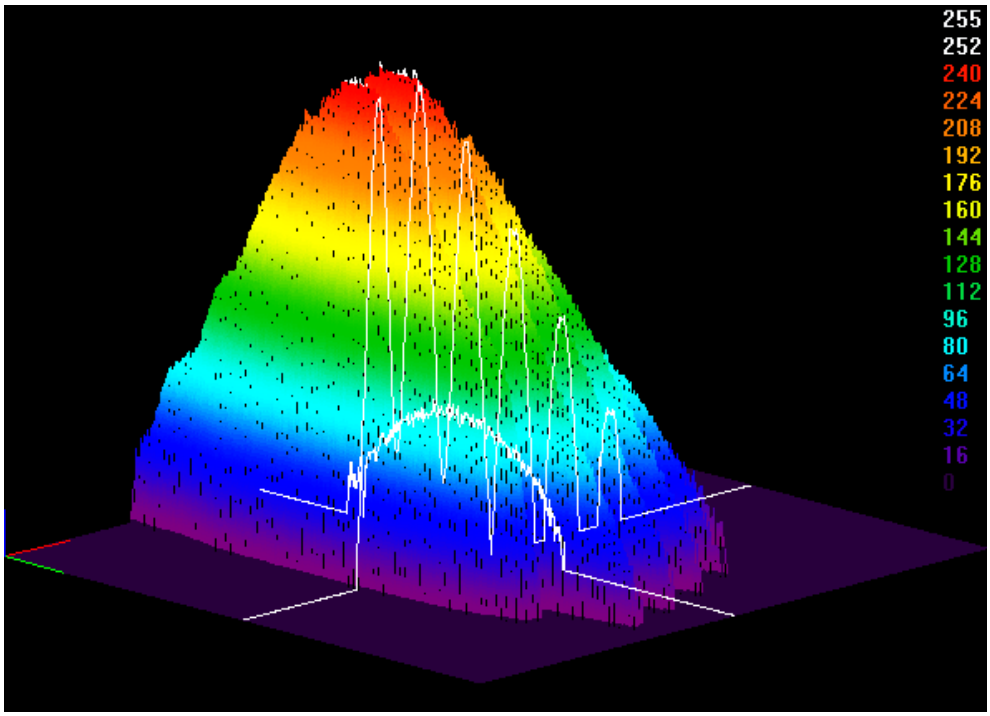

Waveguide 2:

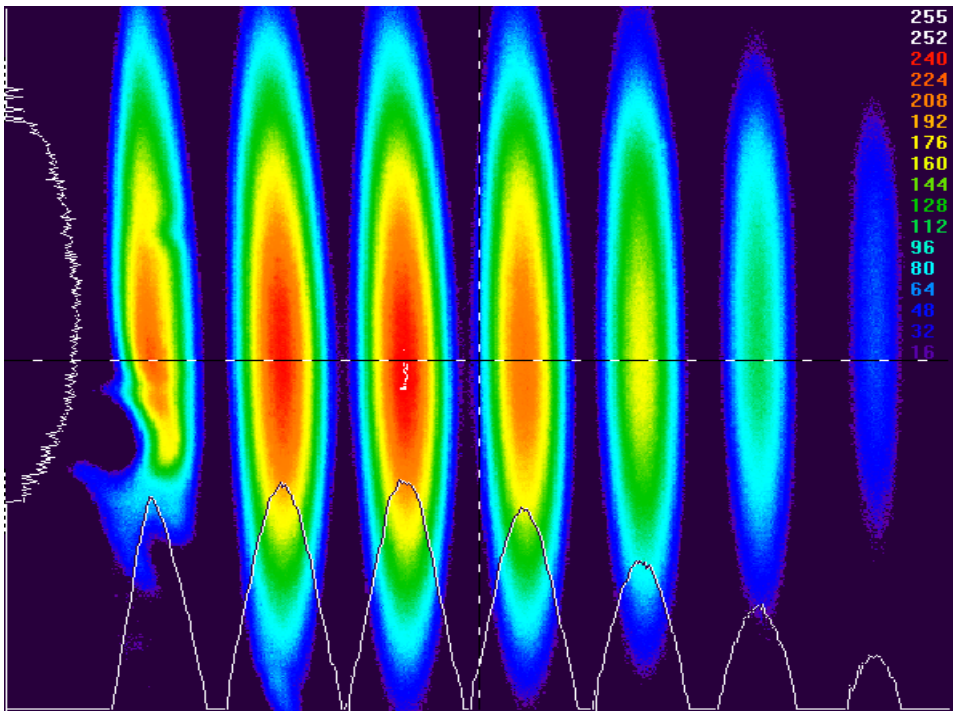
255
252
240
224
208
192
176
160
144
128
112
96
80
64
48
32
16

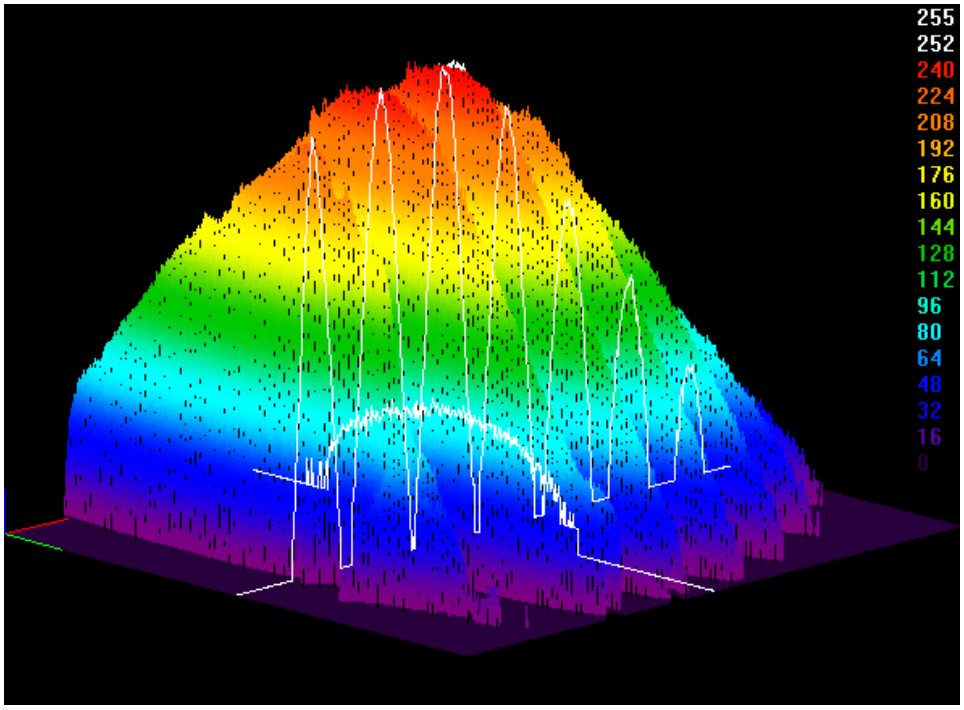
255
252
240
224
208
192
176
160
144
128
112
96
80
64
48
32
16
0

Waveguide 3:

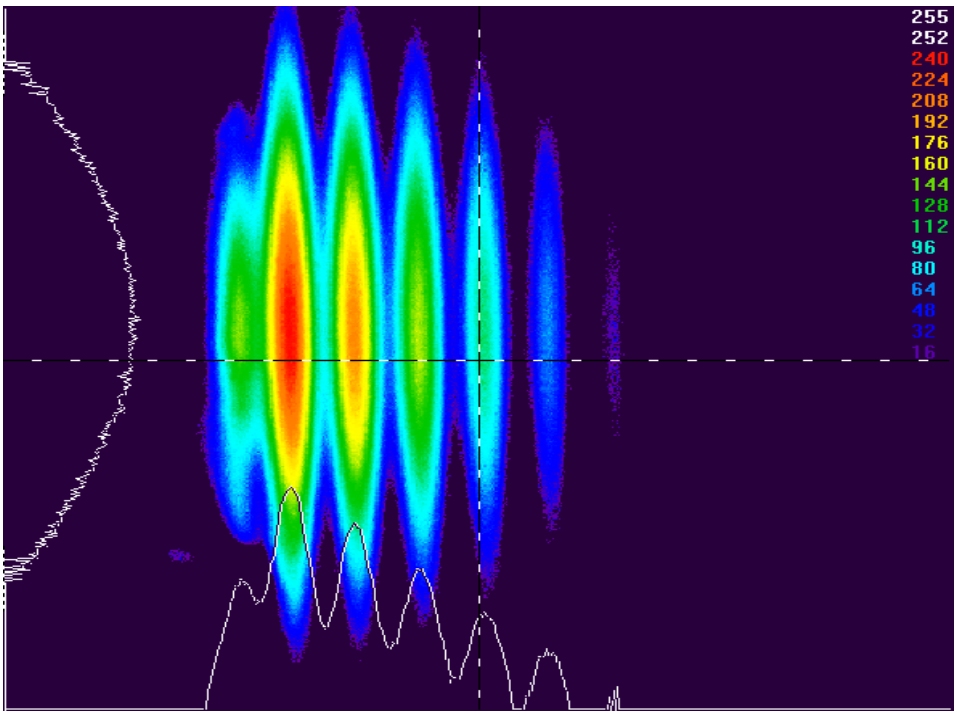
255
252
240
224
208
192
176
160
144
128
112
96
80
64
48
32
16

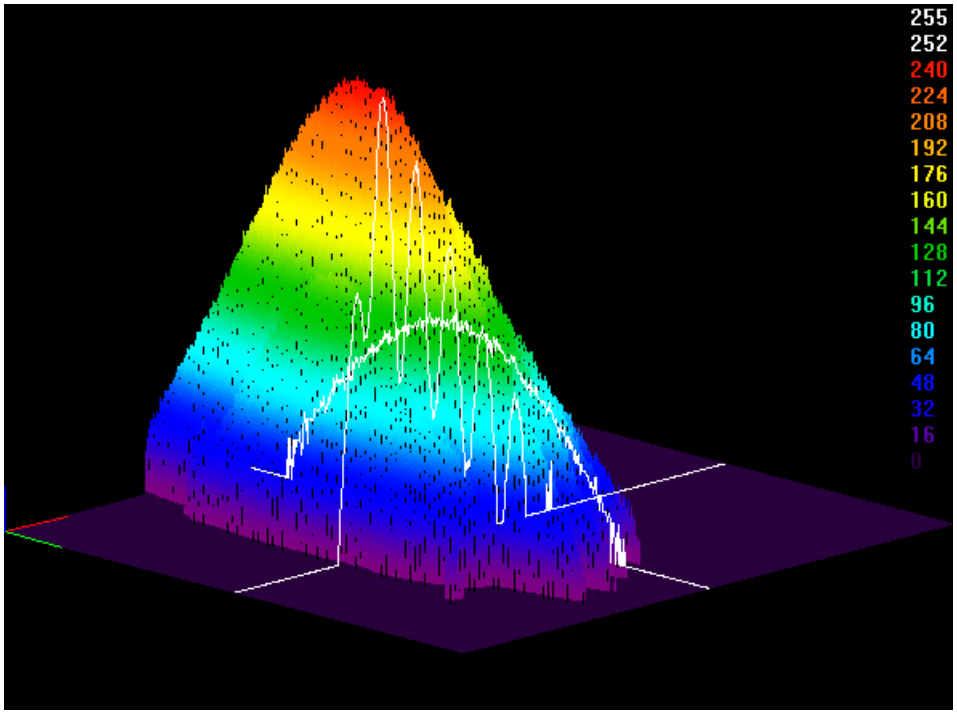
255
252
240
224
208
192
176
160
144
128
112
96
80
64
48
32
16
0

Waveguide 4:

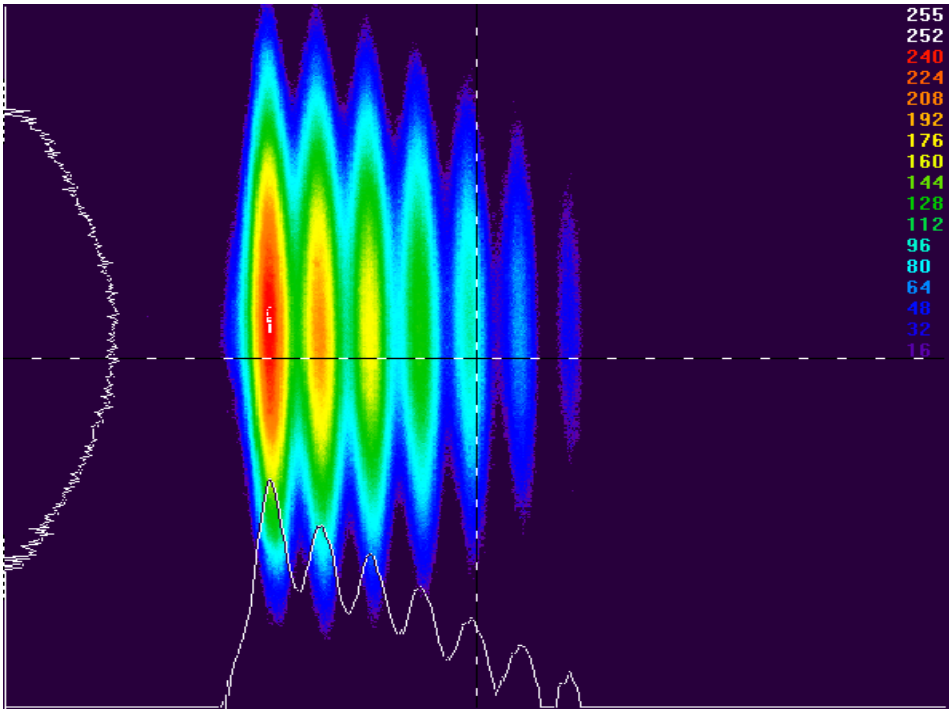
255
252
240
224
208
192
176
160
144
128
112
96
80
64
48
32
16

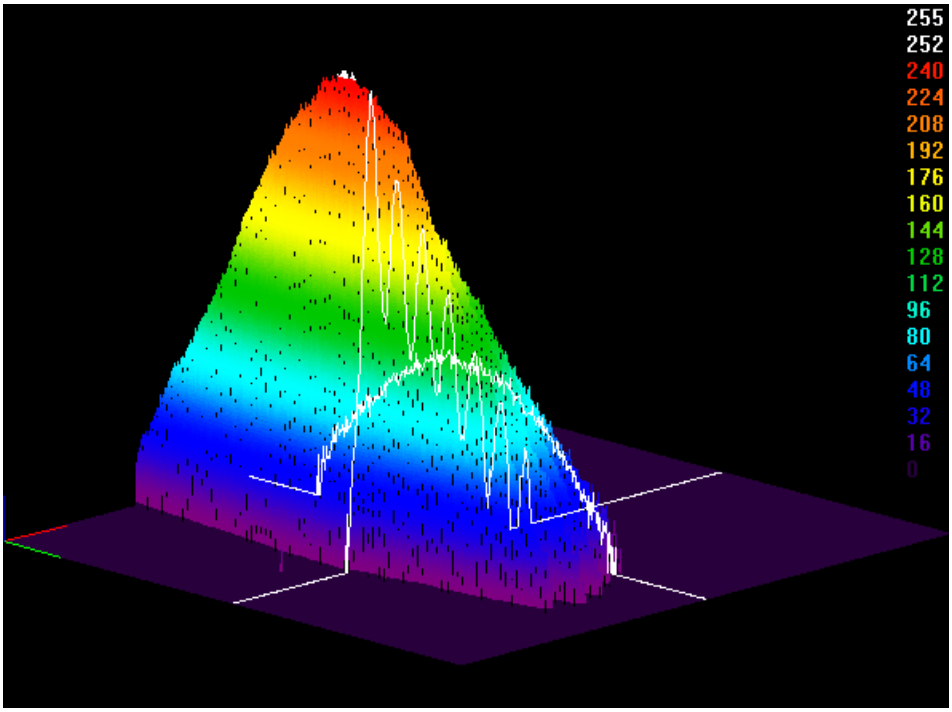
255
252
240
224
208
192
176
160
144
128
112
96
80
64
48
32
16
0

Waveguide 5:

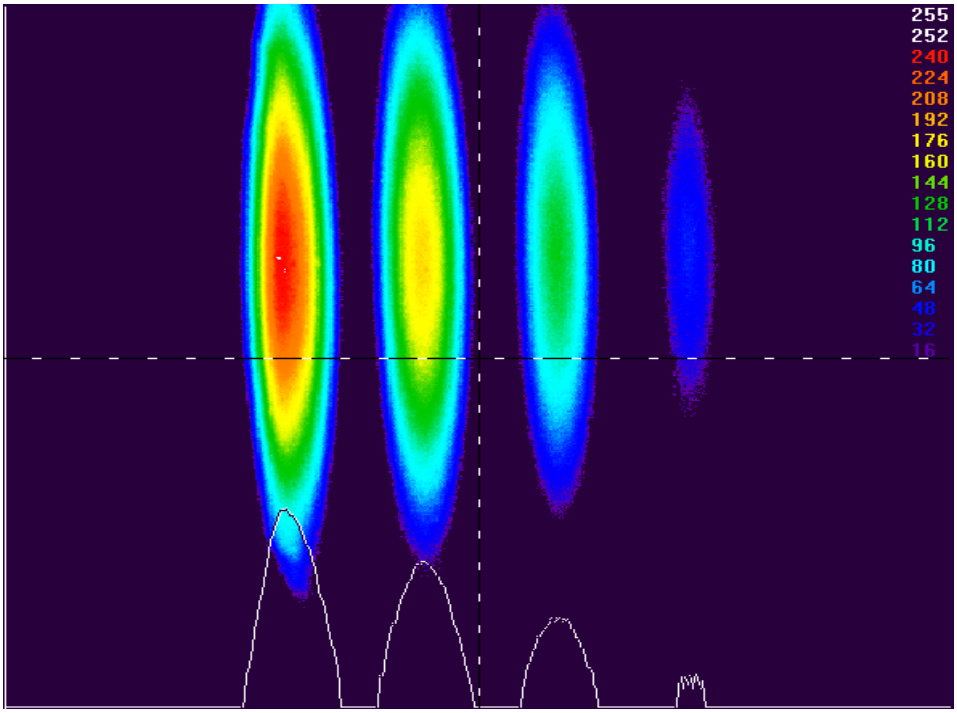
255
252
240
224
208
192
176
160
144
128
112
96
80
64
48
32
16

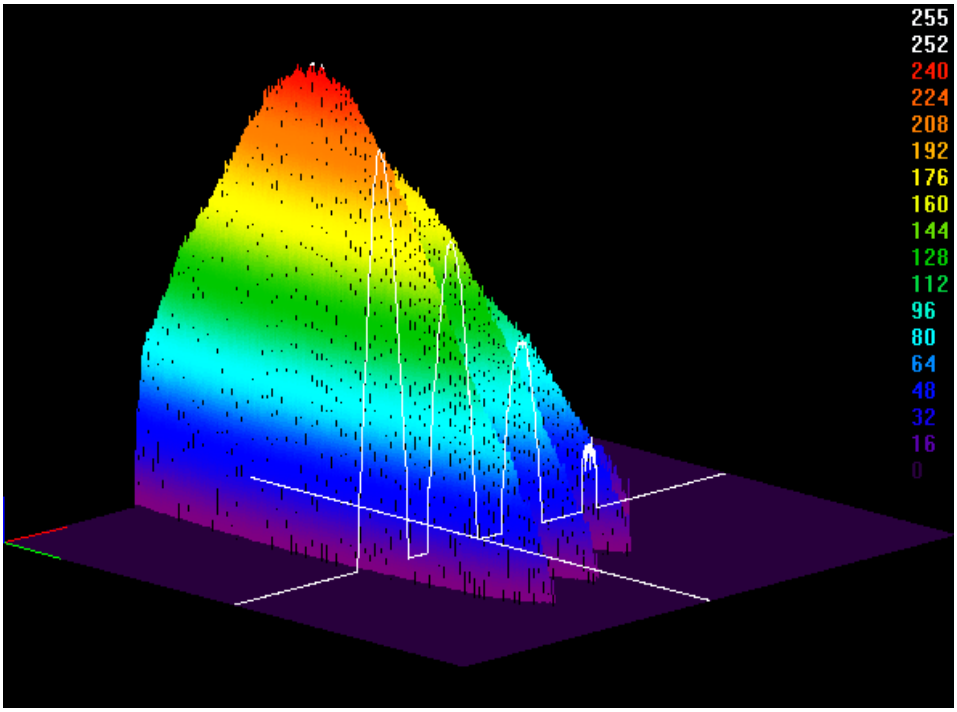
255
252
240
224
208
192
176
160
144
128
112
96
80
64
48
32
16
0

APPENDIX C
CHARACTERIZATION RESULTS WITH FOUNTAIN PEN MICROPATTERNING

Characterization results showing the output power profile of MZI developed using LDW and fountain pen-based micro-patterning.

Waveguide 1:

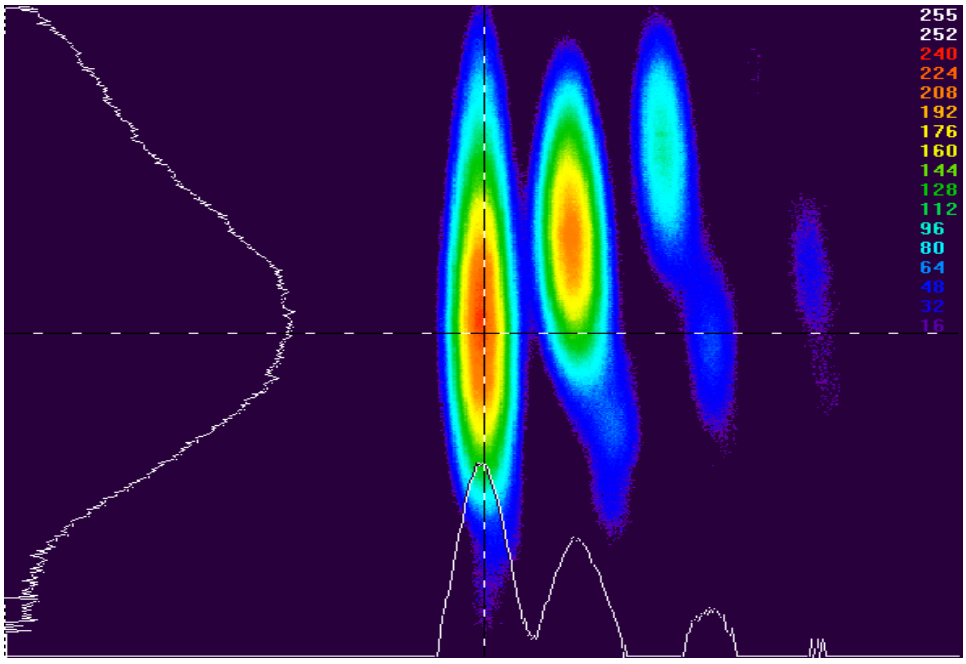

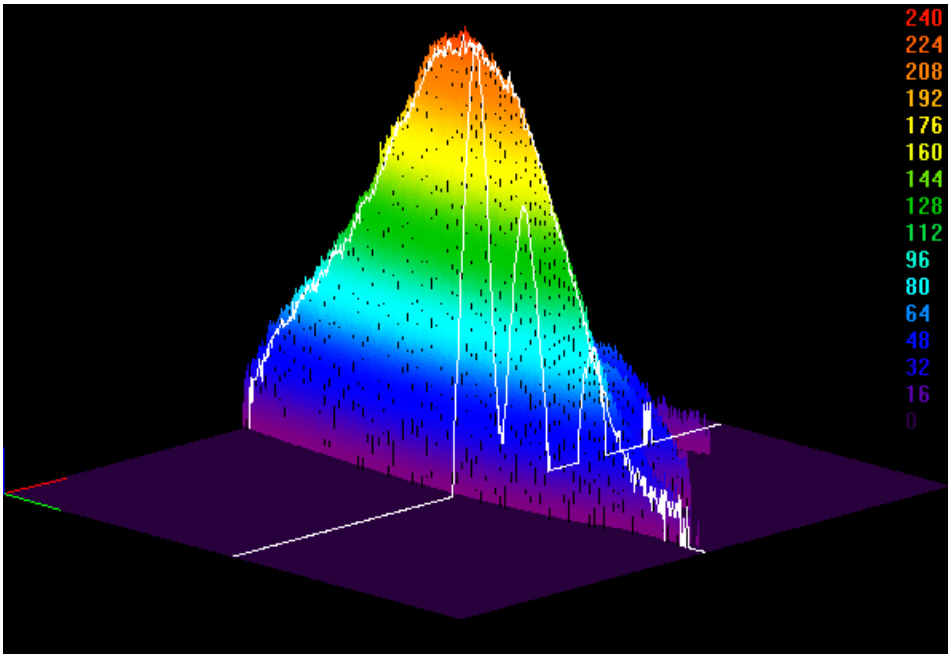

Waveguide 2:

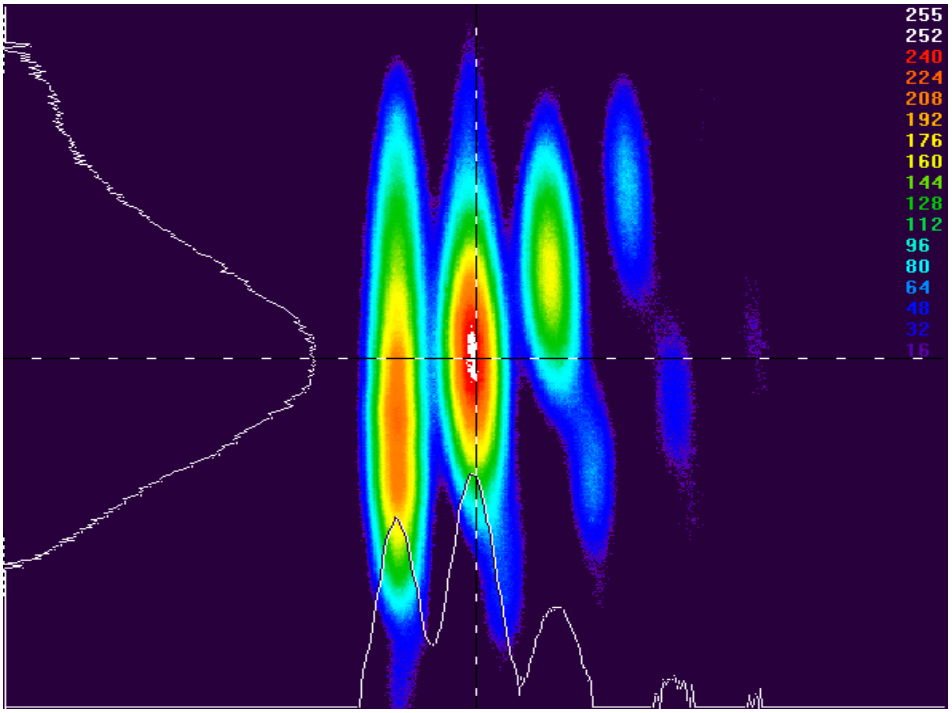
255
252
240
224
208
192
176
160
144
128
112
96
80
64
48
32
16

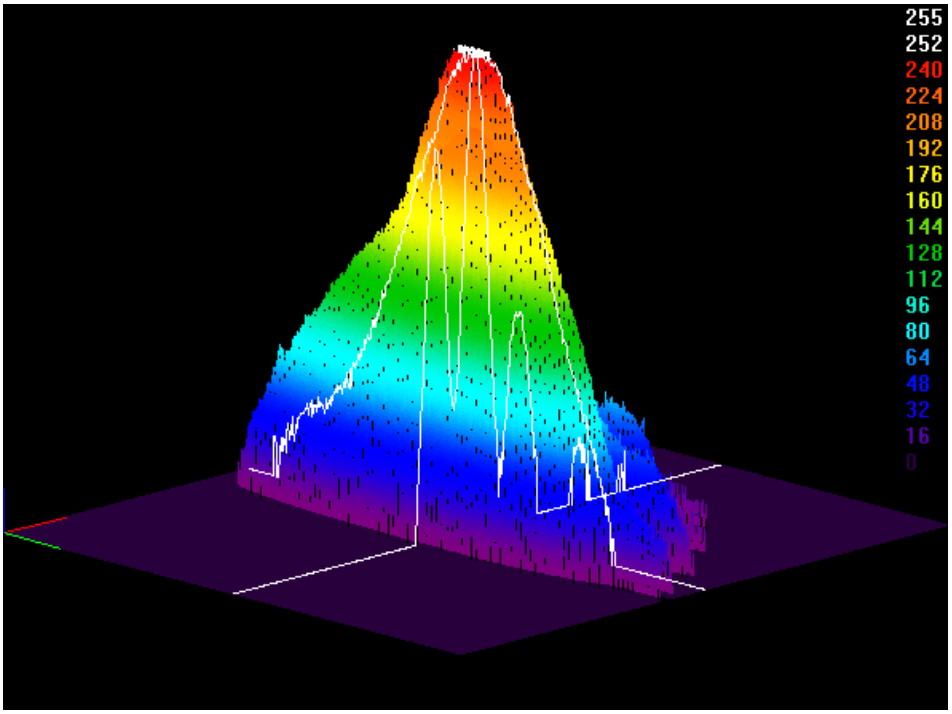
255
252
240
224
208
192
176
160
144
128
112
96
80
64
48
32
16
0

Waveguide 3:

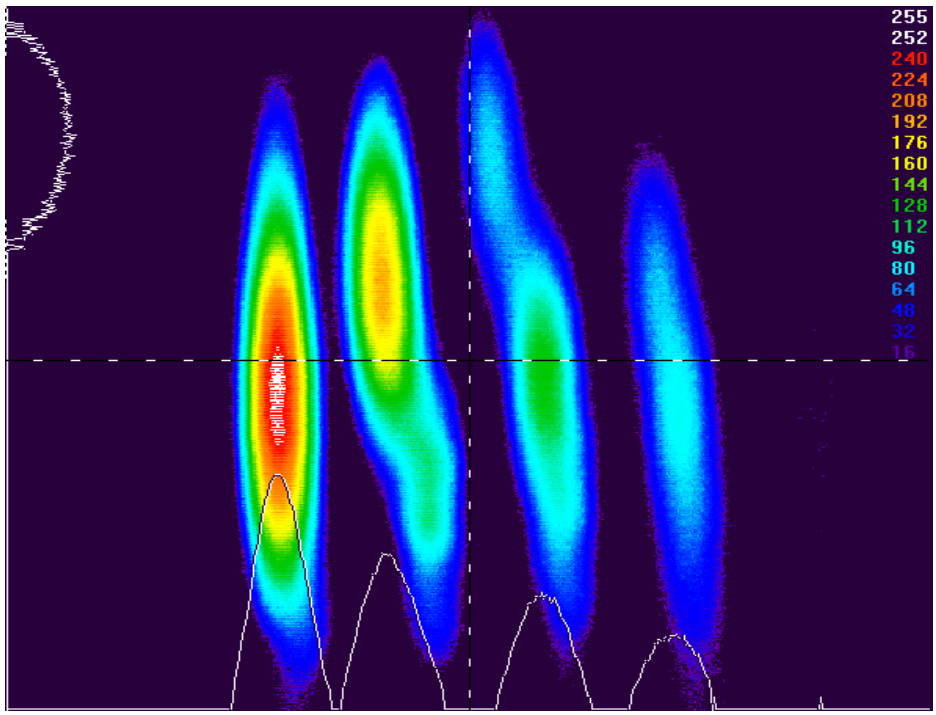
255
252
240
224
208
192
176
160
144
128
112
96
80
64
48
32
16

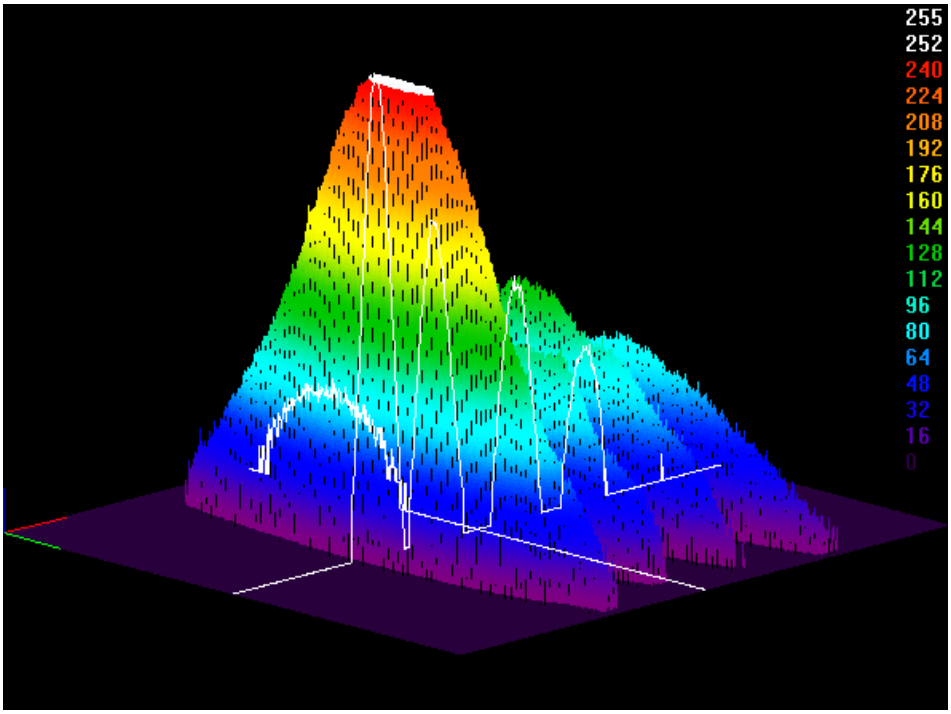
255
252
240
224
208
192
176
160
144
128
112
96
80
64
48
32
16
0

Waveguide 4:

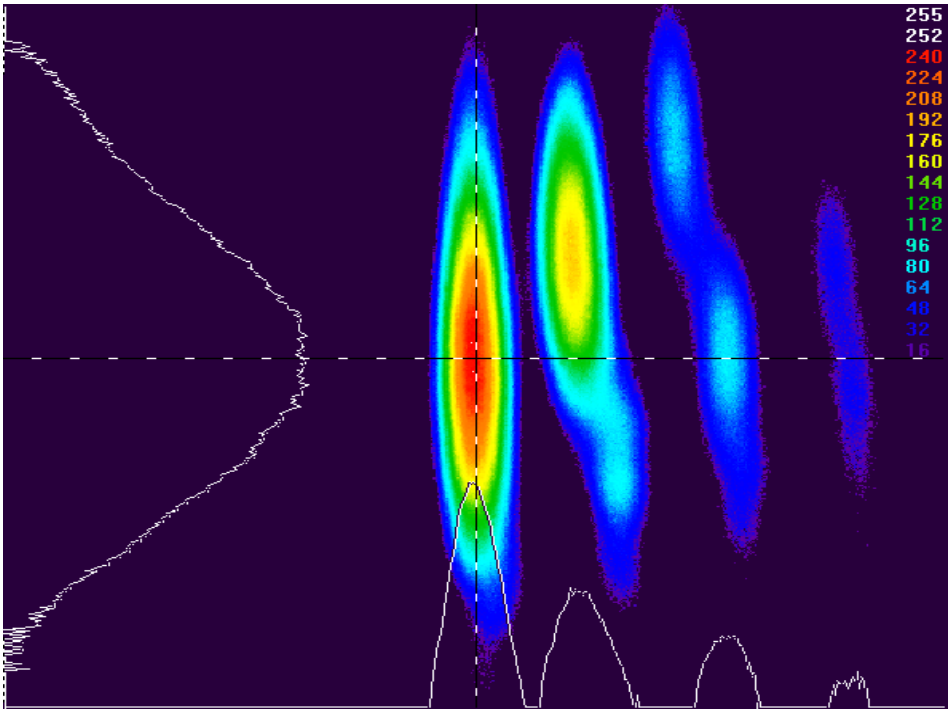
255
252
240
224
208
192
176
160
144
128
112
96
80
64
48
32
16

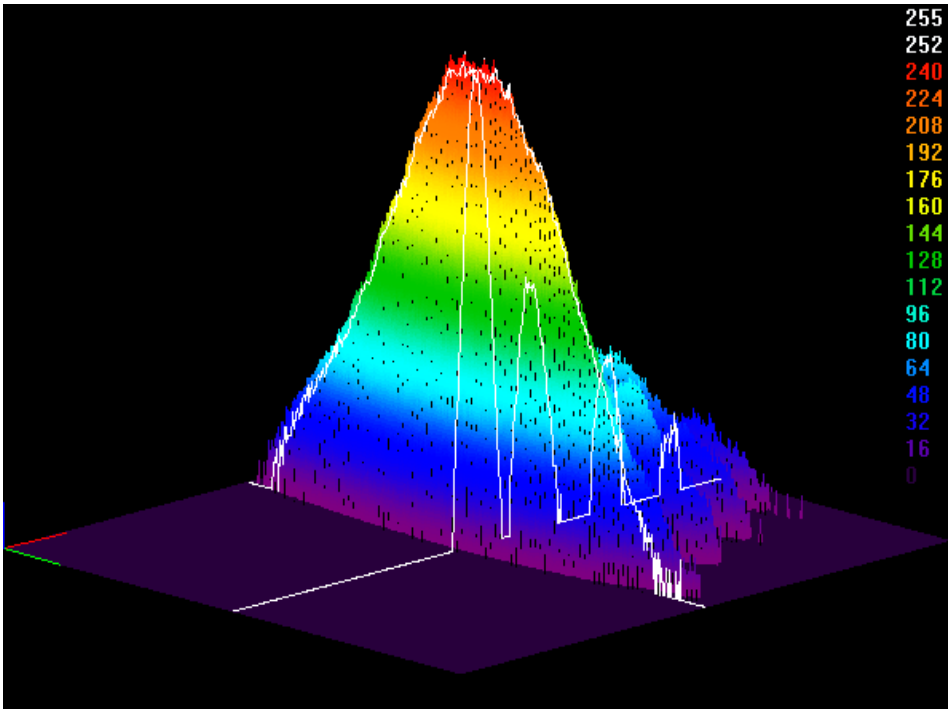
255
252
240
224
208
192
176
160
144
128
112
96
80
64
48
32
16
0

Waveguide 5:

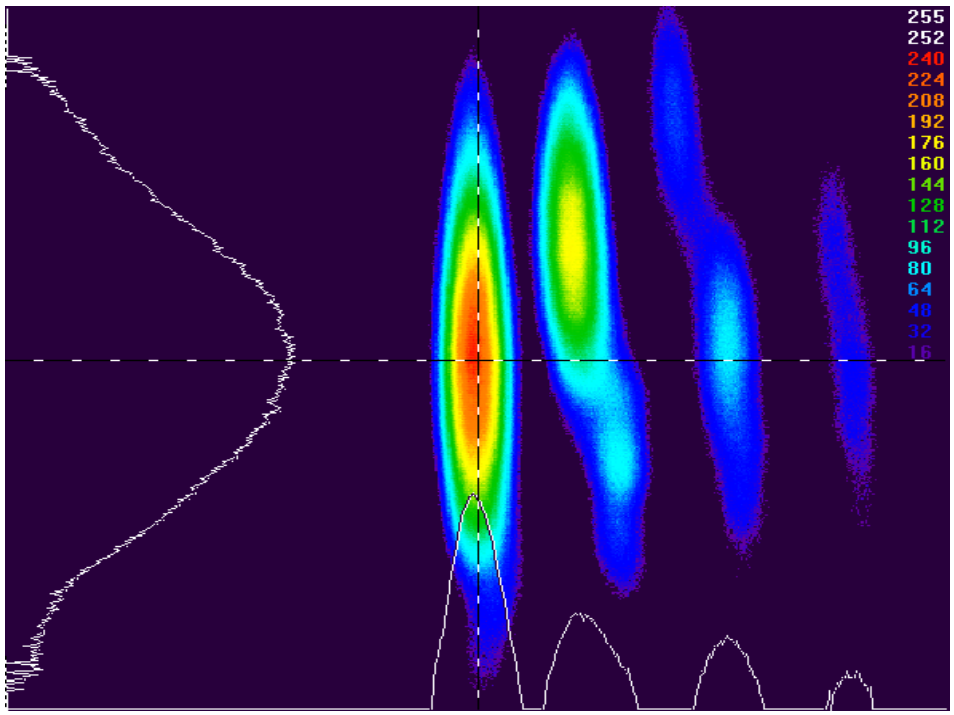
255
252
240
224
208
192
176
160
144
128
112
96
80
64
48
32
16

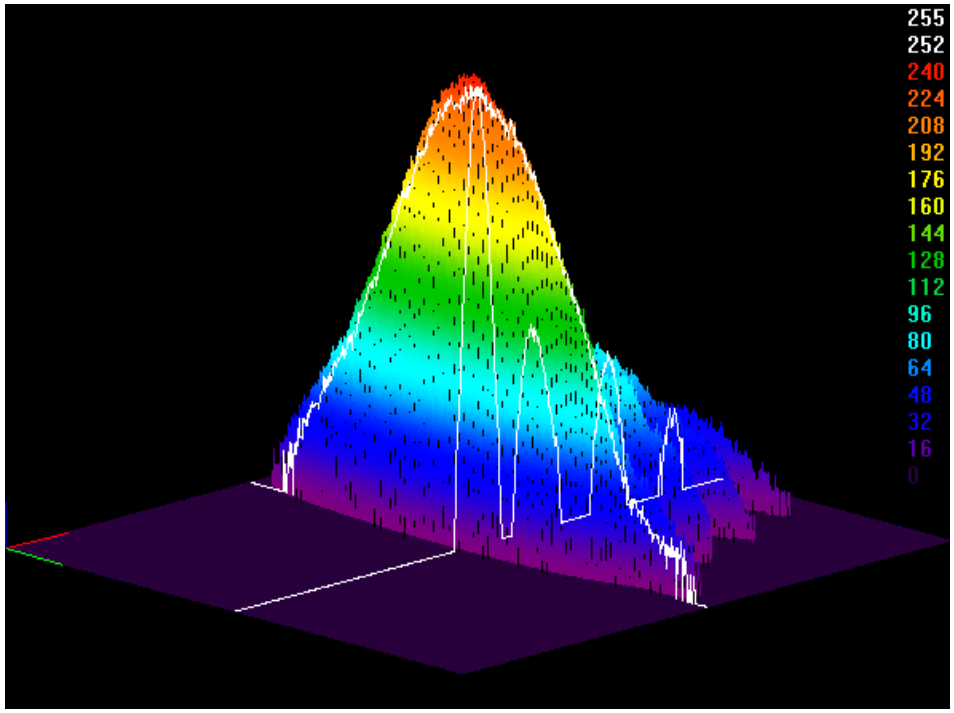
255
252
240
224
208
192
176
160
144
128
112
96
80
64
48
32
16
0

APPENDIX D

CHARACTERIZATION OF PDMS THIN FILMS

A project report on “Spin-Coating Process and Optical Characterization of PDMS Films” submitted to Total Wire Corporation.

Spin-Coating Process and Optical Characterization of PDMS Films

1. Introduction

The optimal parameters for spin-coating the PDMS elastomer on glass substrates and the possible effect of curing process on the refractive index of the thin film have been studied. A variety of solvents has been attempted to dissolve the PDMS, including the following solvents, Toluene, Cyclohexonane cert acs, Cyclohexanone, Chloroform, 1,2 - Dichloromethane, Acetonitrile acs, Benzene acs, Mineral oil, P-Dioxane acs, 1-chloroButane, Nitro Benzene, Methylene Chloride. Only Chloroform, Benzene acs, and Toluene can dissolve PDMS completely. We performed the experiments using these three solvents.

2. Sample Preparation

To prepare a sample of the PDMS thin films following steps were followed during the entire project.

Substrate Preparation

First, substrates were soaked in a Branson optical cleaner solution for 12 hours, followed by 10 minutes in an ultrasonic bath (Branson 2510 Ultrasonic Cleaner) in the cleaner solution. Substrates will then be rinsed thoroughly in deionized water, followed by 10 minutes in an ultrasonic bath in deionized water. Finally, each side was blow-dried using compressed nitrogen and then the substrates are baked in a vacuumed oven at 100° C for 12 hours.

PDMS Solution Preparation

- Take PDMS by weight in grams in a clean bottle.
- Add the curing agent solution to the PDMS in the ratio of 10 parts of PDMS to 1 part of curing agent by weight (10:1). Mix the PDMS and the curing agent.
- Add the solvent to this mixture using a desired ratio. Typical ratios used are 0.5:1, 1:1 and 2:1. Where, 2:1 resembles 2 parts of the solvent to 1 part of PDMS.
- Shake the mixture well so that the solvent dissolves the PDMS completely and a clear mixture solution is seen.
- This solution can now be used to coat thin films on glass or polymer substrates.

Method for Spin Coating PDMS

The PWM32 Photoresist Spinner (Headway Research, Inc.) is used for preparing PDMS thin films. The thin film is coated at various spin speeds and ramping speeds. These parameters and steps are programmed into available

recipes of spin coating setup before spinning the thin films. The following steps are used to prepare the PDMS thin films.

- Place a clean glass slide or substrate on the vacuum chalk.
- Select a particular recipe programmed for spin coating.
- Apply the solution on the glass substrate.
- Start the spin coating.

To create a recipe,

- Select a particular Recipe.
- Select step 1.
- Enter the required Spin Speed.
- Enter the required Ramping speed.
- Enter the desired Spin time.
- Enter the Termination Time (Spin Time).
- End the Recipe.

Method for Measurement of Thickness and Refractive Index

The film thickness and the index of refraction are measured using the Model 2010 prism coupler (Metricon Corp.) which is equipped with two laser sources with wavelengths of 1550nm and 633nm.

3. Chloroform as Solvent

3.1 Thickness and Uniformity Relationship with Spin Speed and Ramping Speed

The PDMS thin films with Chloroform as solvent are prepared using spin speeds of 2000 RPM, 4000 RPM and 6000 RPM. Two concentrations, Chloroform:PDMS = 2:1 and Chloroform:PDMS = 1:1, are used in order to obtain the films with the thickness ranges from approximately 7 to 20 µm. Under each spin speed, the different ramping speeds of 1000, 2000, and 4000 RPM/sec are used to study how spin speed and/or ramping speed affect the film uniformity. The finished films are cured by baking the thin films at 70° C, few degrees above the boiling temperature of the solvent, for 40 minutes.

For each spin speed nine samples are prepared with three samples for each ramping speed. The film thicknesses are measured cross each 1 x 1 inch glass substrate (five readings are taken for each sample). The mean and SD of the measured thickness are calculated and the results are listed in Tables 1 and 2 respectively.

Table 1 The mean and SD of the measured thickness for Chloroform:PDMS = 2:1

Spin Speed (RPS)	Ramping Speed (RPM/s)	Thickness Mean (µm)	SD
2000	1000	13.6859	0.7189
	2000	11.2920	0.6687
	4000	11.2153	0.7100
4000	1000	11.5539	0.2547
	2000	9.8659	0.186
	4000	9.6194	0.2166
6000	1000	9.343	0.1914
	2000	8.6414	0.2689
	4000	7.3246	0.1601

Table 2 The mean and SD of the measured thickness for Chloroform:PDMS = 1:1

Spin Speed (RPS)	Ramping Speed (RPM/s)	Thickness Mean (µm)	SD
2000	1000	19.7785	0.4817
	2000	18.8348	0.1657
	4000	17.3821	0.5498
4000	1000	13.4057	0.0981
	2000	12.3793	0.1915
	4000	11.1293	0.1574
6000	1000	10.8419	0.3682
	2000	10.1293	0.2440
	4000	9.3213	0.1965

Observations

1. As expected, high spin speed results in thinner films.
2. Based on the SD, high spin speeds (4000rpm to 6000rpm) also results in high film uniformity. 2000 rpm spin speed produces poor uniformity.
3. Ramping speed doesn't seem to affect significantly the film uniformity though higher ramping speed yield thinner films.

Refractive Index Measurement

The Refractive index of PDMS thin films is measured and compared by using two different curing processes.

- Baking the thin film at few degrees above the boiling temperature of Chloroform (at 70° C).
- Baking the thin film at 100° C.

Four samples for each curing temperature are prepared for measurement of refractive indices. Tables 3 and 4 are the measurement results and the calculated mean and the SD.

Table 3 Refractive index measurement for samples prepared at 70° C.

Sample	n at 633 nm	n at 1550 nm
1	1.4083	1.3977
2	1.4084	1.3982
3	1.4087	1.4006
4	1.4087	1.3979
Mean	1.4085	1.3986
SD	0.00021	0.00135

Table 4 Refractive index measurement for samples prepared at 100° C.

Sample	n at 633 nm	n at 1550 nm
1	1.4103	1.3992
2	1.4097	1.3981
3	1.4122	1.4034
4	1.4080	1.3983
Mean	1.4101	1.4000
SD	0.001730	0.002480

The Difference of the refractive indices between the thin films when cured at different temperatures is as below,

Mean Difference	
Δn at 633 nm	**Δn at 1550 nm**
0.0015	0.0012

To confirm the above result, four more samples for each curing temperature are prepared under the same condition and the refractive indices are measured.

The difference of the refractive indices between the thin films when cured at different temperatures is as below,

Mean Difference	
Δn at 633 nm	**Δn at 1550 nm**
0.0028	0.0010

Observations

From the above results, it is observed that there is a slight increase in the refractive index of the PDMS thin film with Chloroform as the solvent when cured at higher temperature (0.11% to 0.20% increase at 633nm and 0.07% to 0.09% increase at 1550nm).

4. Benzene as Solvent

4.1 Thickness and Uniformity Relationship with Spin Speed and Ramping Speed

The PDMS thin films with Benzene as solvent are prepared using spin speeds of 2000, 4000, and 6000 RPM. Two concentrations, Benzene:PDMS = 1:1 and Benzene:PDMS = 0.5:1, are used in order to obtain the films with the thickness ranges from approximately 6 to 19 µm. Under each spin speed, the different ramping speeds of 1000, 2000, and 4000 RPM/sec are used to study how spin speed and/or ramping speed affect the film uniformity. The finished films are cured by baking the thin films at 90° C, 10° C above the boiling temperature of the solvent, for 40 minutes.

For each spin speed nine samples are prepared with three samples for each ramping speed. The film thicknesses are measured cross each 1 x 1 inch substrate (five readings are taken for each sample). Mean thickness and SD are calculated and the results are listed in Tables 5 and 6 respectively.

Table 5 The mean and SD of the measured thickness for Benzene:PDMS = 1:1

Spin Speed (RPS)	Ramping Speed (RPM/s)	Thickness Mean (µm)	SD
2000	1000	10.4029	0.1704
	2000	9.0268	0.3961
	4000	9.7564	0.2114
4000	1000	9.0203	0.0816
	2000	7.6313	0.0853
	4000	6.7454	0.1251
6000	1000	7.5549	0.0855
	2000	6.8727	0.1480
	4000	6.0907	0.1242

Table 6 The mean and SD of the measured thickness for Benzene:PDMS = 0.5:1

Spin Speed (RPS)	Ramping Speed (RPM/s)	Thickness Mean (μm)	SD
2000	1000	19.1232	0.1131
	2000	18.6684	0.1096
	4000	16.6316	0.1061
4000	1000	12.8572	0.2194
	2000	12.0506	0.1127
	4000	11.7143	0.2681
6000	1000	9.9231	0.1354
	2000	9.4810	0.1080
	4000	9.0536	0.1651

Observations

1. By comparing the SD of the measured thickness for the PDMS thin films with Chloroform and Benzene as solvents, it can be seen that the uniformity of the thin films with Benzene (relative low evaporation rate) as solvent is better than that with Chloroform (relative high evaporation rate) as solvent.
2. High spin speed results in thinner films.
3. The uniformity of the thin film doesn't have considerable improvement with increased spin speed.
4. Ramping speed doesn't seem to affect significantly film uniformity though higher ramping speed yields thinner films.

Refractive Index Measurement

The refractive index of PDMS thin films is measured and compared by using two different curing processes.

- Baking the thin film at 10° C above the boiling temperature of Benzene (at 90° C).
- Baking the thin film at 30° C above the boiling temperature of Benzene (at 120° C).

Four samples for each curing temperature are prepared for measurement of refractive indices. Tables 7 and 8 are the measurement results and the calculated mean and the SD.

Table 7 Refractive index measurement for samples prepared at 90° C.

Sample	n at 633 nm	n at 1550 nm
1	1.4096	1.3998
2	1.4095	1.3993
3	1.4096	1.3991
4	1.4097	1.3992
Mean	1.4096	1.3994
SD	0.00008	0.00031

Table 8 Refractive index measurement for samples prepared at 120° C.

Sample	n at 633 nm	n at 1550 nm
1	1.4104	1.4005
2	1.4106	1.4001
3	1.4109	1.3995
4	1.4107	1.4006
Mean	1.4107	1.4002
SD	0.00020	0.00050

The Difference between the refractive indices between the thin films when cured at different temperatures is as below,

Mean Difference	
Δn at 633 nm	**Δn at 1550 nm**
0.00105	0.00083

Observations

Similarly to the Chloroform case, from the above results, it is observed that there is an insignificant increase in the refractive index of the PDMS thin film with Benzene as solvent when cured at higher temperature (0.07% increase at 633nm and 0.06% increase at 1550nm).

5. Toluene as Solvent

5.1 Thickness and Uniformity Relationship with Spin Speed and Ramping Speed

The PDMS thin films with Toluene as solvent are prepared using spin speeds of 2000 RPM, 4000 RPM and 6000 RPM. Three concentrations, Toluene:PDMS = 1:1 and Toluene:PDMS = 0.5:1, and Toluene:PDMS = 0.25:1 are used in order to obtain the films with the thickness ranges from approximately 4 to 22 µm. Under each spin speed, the different ramping speeds of 1000, 2000, and 4000 RPM/sec are used to study how spin speed and/or ramping speed affect the film uniformity. The finished films are cured by baking them at 120° C, ten degrees above the boiling temperature of the solvent, for 40 minutes.

For each spin speed nine samples are prepared with three samples for each ramping speed. The film thicknesses are measured cross each 1 x 1 inch glass substrate (five readings are taken for each sample). The mean and SD of the measured thickness are calculated and the results are listed in Tables 1 and 10 respectively.

Table 9 The mean and SD of the measured thickness for Toluene:PDMS = 1:1

Spin Speed (RPS)	Ramping Speed (RPM/s)	Thickness Mean (µm)	SD
2000	1000	7.2152	0.1654
	2000	6.8250	0.2215
	4000	6.7649	0.1336
4000	1000	5.7656	0.1127
	2000	5.0947	0.1771
	4000	4.8648	0.1756
6000	1000	5.3909	0.1106
	2000	4.6913	0.1145
	4000	4.1703	0.1132

Table 10 The mean and SD of the measured thickness for Toluene:PDMS = 0.5:1

Spin Speed (RPS)	Ramping Speed (RPM/s)	Thickness Mean (μm)	SD
2000	1000	13.1695	0.1492
	2000	12.8333	0.1219
	4000	11.1680	0.1832
4000	1000	9.3330	0.0938
	2000	9.1984	0.0843
	4000	8.8807	0.0895
6000	1000	7.9044	0.0875
	2000	7.4335	0.0854
	4000	6.8432	0.0877

Table 11 The mean and SD of the measured thickness for Toluene:PDMS = 0.25:1

Spin Speed (RPS)	Ramping Speed (RPM/s)	Thickness Mean (μm)	SD
2000	1000	22.6366	0.3238
	2000	22.3843	0.2077
	4000	22.0775	0.1189
4000	1000	13.2858	0.1245
	2000	12.7736	0.1079
	4000	12.6343	0.1419
6000	1000	9.6987	0.1364
	2000	9.5631	0.1880
	4000	9.2178	0.2097

Observations

1. By comparing the SD it can be seen that the uniformity of the thin films with Toluene (lowest evaporation rate) as solvent is similar to that with Benzene as solvent.
2. High spin speed results in thinner films.
3. The uniformity of the thin film are not affected significantly by the spin speed or ramping speed except for one case. For Toluene:PDMS = 0.25:1 and low spin speed (2000rpm), the film uniformity tends to be poor especially when ramping speed is low.
4. Higher ramping speed yields thinner films.

5.2. Refractive Index Measurement

The refractive index of PDMS thin films prepared by using two different curing processes is measured and compared.

- Baking the thin film on a hot stage at 120ºC (approximately 10ºC above the boiling temperature of Toluene) for 40 minutes.
- Baking the thin film at 150ºC for 40 minutes.

Four samples for each curing temperature are prepared for measurement of refractive indices. Tables 12 and 13 are the measurement results and the calculated mean and the standard deviation (SD).

Table 12 Refractive index measurement for samples prepared at 120° C.

Sample	n at 633 nm	n at 1550 nm
1	1.4102	1.4001
2	1.4101	1.3997
3	1.4099	1.4003
4	1.4101	1.4003
Mean	1.4101	1.4001
SD	0.00013	0.00028

Table 13 Refractive index measurement for samples prepared at 150° C.

Sample	n at 633 nm	n at 1550 nm
1	1.4101	1.4001
2	1.4104	1.3992
3	1.4101	1.3991
4	1.4100	1.4001
Mean	1.4102	1.3996
SD	0.00017	0.00055

The difference of the refractive indices between the thin films when cured at different temperatures is as below,

Mean Difference	
Δn at 633 nm	**Δn at 1550 nm**
0.000075	-0.000475

Observations

The above result suggests that the change in the curing temperature does not affect the refractive index of the PDMS thin film with Toluene as the solvent.

5. Conclusions

As the result of the experiments we conclude that (1) solvent evaporation rate plays an important role in the thin film preparation. The lower evaporation rate solvent (e.g. Toluene and Benzene) produces more uniform films. The thin films prepared by using the solvent with high evaporation rate (e.g. Chloroform) have poor thickness uniformity, especially when spin speed is low. (2) When film is curried at the temperature that is approximately 30^{o}C above the solvent boiling temperature, insignificant change of the refractive indices is observed (when Chloroform and Benzene are used as solvent). (3) As expected, higher spin speed and higher ramping speed produce thinner films. No strong relationship between spin speeds and film uniformity has been observed when spin speed is high (4000 and 6000 rpm). However, the film uniformity begins to decline when lower spin speed (e.g. 2000rpm) is used.

REFERENCES

[1] Hierlemann A., Brand O., Hagleitner C., Baltes H. “Microfabrication techniques for Chemical/Biosensors” Proceedings of the IEEE 91. no. 6 (2003): 839-63.

[2] Hunsperger R. G. Integrated Optics: Theory and Technology. New York: Springer-Verlag, 2002.

[3] Wong, W., H., and Pun, E. B. Y. “Electron beam direct-write tunable polymeric waveguide grating filter” IEEE Photonics Technol. Lett. 15, no. 12 (2003): 1731-1733.

[4] Vittorio, M. D., Todaro, M.T., Stomeo, T., Cingolani, R., Cojoc, D., and Di Fabrizio, E. “Two-dimensional photonic crystal waveguide obtained by e-beam direct writing of SU8 2000 photoresist” Microelectronic Engin., 73-74 (2004): 388-391.

[5] Chiron, D., Trigaud, T., and Moliton, J. P. “Optical waveguides etched in 6FDA-ODA by focused ion beam,” Synthetic Metals, 124 no. 1 (2001): 33-35.

[6] Eldada, L., Xu, C., Stengel, M. T., Shacklette, L. W., and Yardley, J. T., “Laser fabricated low-loss single mode raised-rib waveguiding devices in polymers” J. Lightwave Technol. 14 no. 7 (1996): 1704-1713.

[7] Wang, S., Borden, B., Li, Y., and Goel, P. “Laser Direct Writing of inorganic-organic hybrid polymeric channel waveguide for optical integrated circuits” Proceedings SPIE. 6389 (2006): 1-7.

[8] Krchnavek, R. R., Lalk, G. R., and Hartman, D. H. “laser direct writing of channel waveguides using spin-on polymers” J. Appl. Phys. 66 (1989): 5156-5160.

[9] Prieto F., Supelveda B., Calle A., Llobera A., Dominquez C., and Lechuga L. M. “Integrated Mach-Zehnder Interferometer based on ARROW structures for biosensor applications” Sensors and Actuators B 92 (2003): 151–158.

[10] Lambeck P. V. “Integrated Optical sensors for the chemical domain” Meas. Sci. Technol. 17 (2006): R93–R116.

[11] Heideman R. G., Kooyman R. P. H. and Greve J. “Performance of a highly sensitive optical waveguide Mach-Zehnder interferometer immunosensor” Sens. Actuators, B10 (1993): 209-217.

[12] Lambeck P. V., Heideman R. G. and Ikkink T. J. “Phase modulated Mach-Zehnder Interferometer for sensor applications” Medical and biological engineering 34 no.1 (1996).

[13] Heideman R. G., Veldhuis G. J., Jager E. W. H. and Lambeck P. V. “Fabrication and packaging of integrated chemo-optical sensors” Sensors and Actuators. B 35-36 (1996): 234-240.

[14] Esinenco D., Psoma S. D., Kusko M., Schneider A. and R. Muller “SU-8 Micro-Biosensor on Mach-Zehnder interferometer” Rev. Adv. Mater. Sci 10 (2005): 295 -299.

[15] Choi Tae Y., Poulikakos D. and Grigoropoulos C. P. “Fountain-pen-based laser microstructuring with gold nanoparticle inks” Applied Physics Letters 85 no. 1(2004).

[16] Fraden J. Handbook of modern Sensors: Physics, designs and applications. New York: Springer-Verlag. 2001.

[17] Harsanyi G. Polymer films in sensor applications: technology, materials, devices and their characteristics. PA: Technomic publication. 1985.

[18] Ridder R., Driessen A., Rikkers E., Lambeck P. V. and Diemeer M. B. J. “design and fabrication of electro-optic polymer modulators and switches” Optical Materials. 12 (1999): 205-214.

[19] Bradenburg A. “Integrated optical Interferometers for refractrometry and chemical sensing” Micro-optical technologies for measurement, sensors and Microsystems. 12-13 (1996): 266-76.

[20] Sum T. C., Bettiol A., Venugopal Rao A., VanKan J. A., Ramam A. and Watt F. “Proton Beam writing of passive polymer optical waveguides” Proceedings of SPIE. 5347 (2004): 160-9.

[21] Tay F. E. H., VanKan J. A., Watt F. and Choong W. O. “A novel micro-machining method for the fabrication of thick film SU-8 embedded micro channels” J. Micromech. Microeng. 11 (2001): 27–32.

[22] Tsai H. C. and Doong R. “Simultaneous determination of pH, urea, acetylcholine and heavy metals using array-based enzymatic optical biosensor” Elseveir Biosensors and Bioelectronics 20 (2005): 1796–1804.

[23] Peter M. L., Ping G., Rastislav L. and Kenneth L. S. “Real-time, multiplexed electrochemical DNA detection using an active complementary metal-oxide-semiconductor biosensor array with integrated sensor electronics”, Elsevier Biosensors and Bioelectronics 24 (2009): 1995–2001.

[24] Feldstein, M.J., Golden J.P., Rowe C.A., MacCraith B.D. and Ligler F.S., “Array biosensor: optical and fluidics systems” Biomedical Microdevices 1. no. 2 (1999): 139-53.

[25] Haowen H., Chaocai H., Yunlong Z., Xiaodong X., Xianyong Y., Pinggui Y. and Zhong C.”A novel label-free multi-throughput optical biosensor based on localized surface plasmon resonance” Elsevier Biosensors and Bioelectronics 24 (2009): 2255–2259.

[26] Cesar E., Candido B., Ignacio R. M., Francisco J. A., Elena V. and Mariano L. “Optical fiber sensing devices based on organic vapor indicators towards sensor array implementation” Elsevier Sensors and Actuators B 137 (2009): 139–146.

[27] Zimmerer C., Braun H. G., Kitsche M., Steiner G., Fedrich S. and Salzer R. “Optical Biosensor array based on natural ion channels” Proceedings of the SPIE 5047 (2003): 403-409.

[28] Zhang L., kwan Y. C., Ya R. C. and Trau D. “PDMS microdevice with built-in optical biosensor array for on-site monitoring of the microenvironment within microchannels” Proceedings of the SPIE 6445. (2007).

[29] White I. M., Hongying Z., Suter J.D. Qveys H., Xudong F. “Liquid core optical ring resonator label-free biosensor array for lab-on-a-chip development” Proceedings of the SPIE 6380. (2006).

[30] Guangwei Y., Lear K. L., Stephens M. D., Dandy D. S. “Initial demonstration of a local, evanescent, array coupled biosensor concept” IEEE Sensors. 2005 (2005): 908-911.

[31] Yuan G., Stephens M. D., Dandy D.S., Gerding J.K., Van Orden A. and Lear K.L. “Local evanescent, array coupled (LEAC) biosensor response to low index adlayers”, conference on lasers and electro-optics and 2006 quantum electronics and laser science conference. CLEO/QELS 2006. (2006).

[32] Fanny V., Thierry L., Cedric A., Christian B., Liviu N. and Karsten H., “Direct Patterning of Molecularly Imprinted Microdot Arrays for Sensors and Biochips” Langmuir 23 (2007): 6490-6493.

[33] Yeh, P., “Optical Waves in Layered Media” NY: John Wiley and Sons, Inc., (1988): 70-76.

[34] Heideman, R. G., and Lambeck, P. V. “Remote opto-chemical sensing with extreme sensitivity: design, fabrication and performance of a pig-tailed integrated optical phase-modulated Mach-Zehnder interferometer system” Sens. ActuatorsB61. (1999): 100-127.

[35] Beche B., Pelletier N., Gaviot E., Hierle A., Goullet A., Landesman J. P. and Zyss J “Conception of optical integrated circuits on polymers” Microelectronics Journal 37 (2006): 421–427.

[36] Microchem Inc. “SU-8 2000 Datasheet.” Available from http://www.microchem.com/products/pdf/SU-82000DataSheet2000_5thru2015Ver4.pdf. Internet; accessed 14 April 2009.

[37] Norlan Products Inc. “Properties of Norland Optical Adhesive 61.” Available from https://www.norlandprod.com/adhesives/NOA%2061.html. Internet; accessed 14 April 2009.

[38] Rsoft Design Group, “Rsoft CAD user guide” Rsoft Design Group, Inc. 6 1993-2005.

[39] Rsoft Design Group, “BeamPROP user guide” Rsoft Design Group, Inc. 6 1993-2005.

[40] Metricon Corporation. Thin film thickness/Refractive index measurement system operation and maintenance guide – windows program. New Jersey: Metricon Corporation 2003.

[41] Aerotech Inc. The Unidex 600 series CNC programming manual. PA: Aerotech Inc. 2000.

[42] Spiricon Inc. Laser Beam Analyzer for models LBA 700/708/710/712/714PC. UT: Spiricon Inc. 2005.

[43] Nikon Inc. NIS-Elements basic research users’ guide. NY: Nikon Inc. 2000.